Supplement of Atmos. Chem. Phys., 26, 8425–8453, 2026
https://doi.org/10.5194/acp-26-8425-2026-supplement

Atmospheric Chemistry and Physics
Open Access
EGU

Supplement of

Gas-particle partitioning, molecular weight, and yield of organic nitrate under different urban VOC, NO_x, and oxidation conditions during SAPHIR-CHANEL campaign

Farhan R. Nursanto et al.

Correspondence to: Farhan R. Nursanto (farhan.nursanto@wur.nl) and Juliane L. Fry (juliane.fry@wur.nl)

S1 Experimental conditions

The VOC precursor mixture injected in each experiment is a replica of emissions from various urban emission sources based on previous studies, where a selection of compounds is used to represent these emissions. This emission fingerprint is discussed further in Wu et al. (2026). The mixing ratio of expected injected VOCs, the percentage of consumed VOCs, and the expected mixing ratio of consumed VOCs are listed in Tables S1, S2, S3, S4, and S5. To note, the mixing ratios of injected and consumed VOCs are the expected mixing ratios based on the injection and are not verified by observation. The percentage of consumed VOCs is estimated based on the concentration decrease of a specific VOC from observations using GC-TD-FID/MS, or the signal decrease of mass with the same chemical formula as the VOC injected from observations using NH_4^+-Vocus, amine-ToF, and MR-CIMS. The signal decrease may include multiple isomer compounds or by product of reactions in the gas phase, and thus only gives us an estimate. The percentage of consumed compounds where the signal decrease is unavailable is determined by using the value or average of signal decrease from other compounds with similar structure and/or other experiments with similar conditions. In the tables, the percentages are labeled with a superscript uppercase letter if the percentage is obtained from direct observation of the experiment, and labeled with a superscript lowercase letter if the percentage is determined from other compounds/experiments (see the footnote of each table for the meaning of each letter). Examples of sequences in a chamber experiment, which visualize the time series of VOC injection, VOC consumption, the amount of organic aerosol (OA) formed, as well as organic nitrate (ON) in the gas phase (gON) and in the particle phase (pON) are given in Fig. S1.

Table S1. List of injected VOCs for experiments using limonene (single-compound injection) and the cooking emission replica as precursors. The mixing ratio of expected injected VOCs (inj., in ppb), the percentage of consumed VOCs (% cons.), and the mixing ratio of expected consumed VOCs (cons., in ppb) are listed. The percentage of consumed VOCs is based on the concentration decrease or signal decrease of mass from observations (labeled with superscript uppercase letter, see footnote). Compounds with unavailable information of signal decrease use the value or average from other compounds with similar structure and/or other experiments with similar conditions (labeled with superscript lowercase letter, see footnote).

VOC	Formula	limonene (single-compound)						cooking emission					
		daytime low NO			nighttime			daytime low NO			daytime medium NO		
		inj. (ppb)	% cons.	cons. (ppb)	inj. (ppb)	% cons.	cons. (ppb)	inj. (ppb)	% cons.	cons. (ppb)	inj. (ppb)	% cons.	cons. (ppb)
Aldehydes (saturated and unsaturated)													
acetaldehyde	C_2H_4O	-	-	-	-	-	-	7.63	47 %[a]	3.60	7.63	47 %[a]	3.60
propanal	C_3H_6O	-	-	-	-	-	-	9.61	91 %[b]	8.78	9.61	91 %[b]	8.78
pentenal	C_5H_8O	-	-	-	-	-	-	2.41	92 %[M]	2.22	2.41	97 %[M]	2.35
hexadienal	C_6H_8O	-	-	-	-	-	-	4.18	92 %[M]	3.85	4.18	99 %[M]	4.16
heptanal	$C_7H_{14}O$	-	-	-	-	-	-	1.79	47 %[N]	0.83	1.79	82 %[N]	1.47
octenal	$C_8H_{14}O$	-	-	-	-	-	-	0.81	72 %[M]	0.58	0.81	90 %[M]	0.73
nonanal	$C_9H_{18}O$	-	-	-	-	-	-	0.70	93 %[M]	0.66	0.70	99 %[M]	0.70
decanal	$C_{10}H_{20}O$	-	-	-	-	-	-	0.96	51 %[N]	0.49	0.96	88 %[N]	0.85
tridecanal	$C_{13}H_{26}O$	-	-	-	-	-	-	0.04	51 %[c]	0.02	0.04	88 %[c]	0.04
Isoprene, terpenes, and terpenoids													
limonene	$C_{10}H_{16}$	23.00	100 %[M]	22.90	9.00	90 %[M]	8.11	0.35	100 %[G]	0.35	0.35	100 %[G]	0.35
Alcohols, ethers, amines, and others													
ethanol	C_2H_6O	-	-	-	-	-	-	14.03	17 %[N]	2.40	14.03	38 %[N]	5.27
	Summary	**23.00**	**100 %**	**22.90**	**9.00**	**90 %**	**8.11**	**42.53**	**56%**	**23.78**	**42.53**	**67 %**	**28.30**

[a] Value of the compound from the daytime medium NO gasoline emission experiment (see Table S3).
[b] Value of the compound from the daytime low NO future city anthropogenic+biogenic emission replica experiment (see Table S4).
[c] Value of decanal from the same experiment.
[G] Observed signal decrease from GC-TD-FID/MS.
[M] Observed signal decrease from MR-CIMS (benzene reagent).
[N] Observed signal decrease from NH_4^+-Vocus.

Table S2. List of injected VOCs for experiments using the volatile chemical products (VCPs) emission replica as precursor. The mixing ratio of expected injected VOCs (inj., in ppb), the percentage of consumed VOCs (% cons.), and the mixing ratio of expected consumed VOCs (cons., in ppb) are listed. The percentage of consumed VOCs is based on the concentration decrease or signal decrease of mass from observations (labeled with superscript uppercase letter, see footnote). Compounds with unavailable information of signal decrease use the value or average from other compounds with similar structure and/or other experiments with similar conditions (labeled with superscript lowercase letter, see footnote).

VOC	Formula	VCPs											
		daytime low NO			daytime medium NO			daytime high NO			nighttime		
		inj. (ppb)	% cons.	cons. (ppb)	inj. (ppb)	% cons.	cons. (ppb)	inj. (ppb)	% cons.	cons. (ppb)	inj. (ppb)	% cons.	cons. (ppb)
Alkanes													
isobutane	C_4H_{10}	10.50	18 %^{G}	1.90	23.00	18 %^{a}	4.16	23.00	18 %^{a}	4.16	11.00	17 %^{G}	1.86
dodecane	$C_{12}H_{26}$	12.82	37 %^{G}	4.76	11.84	37 %^{a}	4.40	11.51	37 %^{a}	4.27	5.88	16 %^{G}	0.93
octadecane	$C_{18}H_{38}$	0.51	37 %^{b}	0.19	0.47	37 %^{b}	0.18	0.46	37 %^{b}	0.17	0.23	16 %^{b}	0.04
Aromatics													
toluene	C_7H_8	5.21	42 %^{M}	2.20	4.82	59 %^{M}	2.82	4.68	45 %^{M}	2.10	2.39	28 %^{M}	0.68
m-xylene	C_8H_{10}	7.04	59 %^{M}	4.12	6.50	75 %^{M}	4.87	6.32	71 %^{M}	4.46	3.23	22 %^{M}	0.71
Isoprene, terpenes, and terpenoids													
limonene	$C_{10}H_{16}$	3.16	100 %^{G}	3.16	2.92	100 %^{a}	2.92	2.83	100 %^{a}	2.83	1.45	100 %^{G}	1.45
α-pinene	$C_{10}H_{16}$	0.45	73 %^{G}	0.33	0.41	73 %^{a}	0.30	0.40	73 %^{a}	0.29	0.21	63 %^{G}	0.13
β-pinene	$C_{10}H_{16}$	0.45	91 %^{G}	0.41	0.41	91 %^{a}	0.38	0.40	91 %^{a}	0.36	0.21	100 %^{G}	0.21
Alcohols, ethers, amines, and others													
ethanol	C_2H_6O	92.36	24 %^{a}	22.01	85.31	24 %^{a}	20.33	82.92	24 %^{N}	19.76	42.37	24 %^{a}	10.10
ethylene glycol	$C_2H_6O_2$	5.39	13 %^{a}	0.72	4.98	13 %^{a}	0.66	4.84	13 %^{N}	0.64	2.47	13 %^{a}	0.33
ethanolamine	C_2H_7NO	1.92	3 %^{A}	0.05	1.77	3 %^{a}	0.05	1.72	3 %^{a}	0.05	0.88	3 %^{a}	0.02
isopropyl alcohol	C_3H_8O	41.26	32 %^{a}	13.05	38.11	32 %^{a}	12.05	37.05	32 %^{N}	11.72	18.93	32 %^{a}	5.99
propylene glycol	$C_3H_8O_2$	21.11	36 %^{a}	7.58	19.50	36 %^{a}	7.00	18.95	36 %^{N}	6.80	9.68	36 %^{a}	3.48
tetrahydrofuran	C_4H_8O	1.73	37 %^{a}	0.64	1.60	37 %^{a}	0.59	1.55	37 %^{N}	0.58	0.79	37 %^{a}	0.29
2-butoxyethanol	$C_6H_{14}O_2$	0.86	63 %^{a}	0.54	0.79	58 %^{N}	0.46	0.77	68 %^{N}	0.52	0.39	63 %^{a}	0.25
carbitol	$C_6H_{14}O_3$	0.62	80 %^{a}	0.50	0.58	77 %^{N}	0.45	0.56	82 %^{N}	0.46	0.29	80 %^{a}	0.23
triethanolamine	$C_6H_{15}NO_3$	0.36	3 %^{c}	0.01	0.33	3 %^{c}	0.01	0.32	3 %^{c}	0.01	0.16	3 %^{c}	0.005
D5-siloxane	$C_{10}H_{30}O_5Si_5$	1.39	17 %^{a}	0.24	1.28	19 %^{N}	0.25	1.25	15 %^{N}	0.19	0.64	17 %^{a}	0.11
	Summary	**207.13**	**30 %**	**62.40**	**204.63**	**30 %**	**61.87**	**199.54**	**30 %**	**59.39**	**101.20**	**26 %**	**26.79**

[a] Value or average value of the compound from the other daytime VCPs experiment(s) with available observation.
[b] Value of dodecane from the same experiment.
[c] Value of ethanolamine from the same experiment.
[A] Observed signal decrease from amine-ToF.
[G] Observed signal decrease from GC-TD-FID/MS.
[M] Observed signal decrease from MR-CIMS (benzene reagent).
[N] Observed signal decrease from NH_4^+-Vocus.

Table S3. List of injected VOCs for experiments using the traffic emission replica (diesel and gasoline) as precursors. The mixing ratio of expected injected VOCs (inj., in ppb), the percentage of consumed VOCs (% cons.), and the mixing ratio of expected consumed VOCs (cons., in ppb) are listed. The percentage of consumed VOCs is based on the concentration decrease or signal decrease of mass from observations (labeled with superscript uppercase letter, see footnote). Compounds with unavailable information of signal decrease use the value or average from other compounds with similar structure and/or other experiments with similar conditions (labeled with superscript lowercase letter, see footnote).

VOC	Formula	diesel emission						gasoline emission					
		daytime medium NO			daytime high NO			daytime medium NO			daytime high NO		
		inj. (ppb)	% cons.	cons. (ppb)	inj. (ppb)	% cons.	cons. (ppb)	inj. (ppb)	% cons.	cons. (ppb)	inj. (ppb)	% cons.	cons. (ppb)
Aldehydes (saturated and unsaturated)													
acetaldehyde	C_2H_4O	-	-	-	-	-	-	2.10	47 %[N]	0.99	2.10	47 %[a]	0.99
acrolein	C_3H_4O	0.67	13 %[N]	0.09	0.67	27 %[N]	0.18	-	-	-	-	-	-
propanal	C_3H_6O	2.94	91 %[b]	2.68	2.94	91 %[b]	2.68	-	-	-	-	-	-
methacrylaldehyde	C_4H_6O	0.47	20 %[c]	0.09	0.47	20 %[c]	0.09	-	-	-	-	-	-
Alkanes													
2-methylbutane	C_5H_{12}	-	-	-	-	-	-	4.35	18 %[d]	0.79	4.35	18 %[d]	0.79
dodecane	$C_{12}H_{26}$	7.48	37 %[e]	2.78	7.48	37 %[e]	2.78	3.33	37 %[e]	1.24	3.33	37 %[e]	1.24
octadecane	$C_{18}H_{38}$	0.58	37 %[f]	0.22	0.58	37 %[f]	0.22	-	-	-	-	-	-
nonadecane	$C_{19}H_{40}$	0.58	37 %[f]	0.22	0.58	37 %[f]	0.22	-	-	-	-	-	-
eicosane	$C_{20}H_{42}$	0.70	37 %[f]	0.26	0.70	37 %[f]	0.26	-	-	-	-	-	-
heneicosane	$C_{21}H_{44}$	0.38	37 %[f]	0.14	0.38	37 %[f]	0.14	-	-	-	-	-	-
docosane	$C_{22}H_{46}$	0.24	37 %[f]	0.09	0.24	37 %[f]	0.09	-	-	-	-	-	-
Alkenes													
ethylene	C_2H_4	11.10	36 %[g]	4.03	11.10	36 %[g]	4.03	11.00	36 %[g]	3.99	11.00	36 %[g]	3.99
1-propene	C_3H_6	4.45	66 %[g]	2.96	4.45	66 %[g]	2.96	6.00	66 %[g]	3.99	6.00	66 %[g]	3.99
1,3-butadiene	C_4H_6	-	-	-	-	-	-	1.00	100 %[h]	1.00	1.00	100 %[h]	1.00
trans-2-butene	C_4H_8	-	-	-	-	-	-	1.00	83 %[g]	0.83	1.00	83 %[g]	0.83
isobutene	C_4H_8	-	-	-	-	-	-	1.50	71 %[g]	1.07	1.50	71 %[g]	1.07
cyclopentene	C_5H_8	0.16	71 %[i]	0.11	0.16	71 %[i]	0.11	-	-	-	-	-	-
cis-2-pentene	C_5H_{10}	-	-	-	-	-	-	0.21	92 %[g]	0.19	0.21	92 %[g]	0.19
Aromatics													
benzene	C_6H_6	-	-	-	-	-	-	1.37	64 %[k]	0.88	1.37	66 %[k]	0.90
toluene	C_7H_8	-	-	-	-	-	-	2.03	64 %[M]	1.29	2.03	66 %[M]	1.33
o-xylene	C_8H_{10}	-	-	-	-	-	-	0.74	84 %[M]	0.62	0.74	87 %[M]	0.64
m-xylene	C_8H_{10}	-	-	-	-	-	-	1.00	84 %[M]	0.84	1.00	87 %[M]	0.87
p-xylene	C_8H_{10}	-	-	-	-	-	-	1.00	84 %[M]	0.84	1.00	87 %[M]	0.87
1,2,4-trimethylbenzene	C_9H_{12}	-	-	-	-	-	-	0.49	18 %[M]	0.09	0.49	9 %[M]	0.04
1,3,5-trimethylbenzene	C_9H_{12}	1.18	57 %[M]	0.67	1.18	48 %[M]	0.57	-	-	-	-	-	-
Alcohols, ethers, amines, and others													
ethanol	C_2H_6O	-	-	-	-	-	-	5.50	33 %[N]	1.83	5.50	33 %[a]	1.83
	Summary	**30.93**	**46 %**	**14.33**	**30.93**	**46 %**	**14.33**	**42.62**	**48 %**	**20.47**	**42.62**	**48 %**	**20.56**

[a] Value of the compound from the daytime medium NO gasoline emission experiment.
[b] Value of the compound from the daytime low NO future city anthropogenic+biogenic emission replica experiment (see Table S4).
[c] Average value of acrolein from the diesel emission experiments.
[d] Value of isobutane from the daytime low NO VCPs experiment (see Table S2).
[e] Value of the compound from the daytime low NO VCPs experiment (see Table S2).
[f] Value of dodecane from the same experiment.
[g] Value of the compound from the daytime low NO Los Angeles anthropogenic emission replica experiment (see Table S4).
[h] Value of the compound from the daytime high NO Los Angeles anthropogenic+biogenic emission replica experiment (see Table S5).
[i] Value of isobutene from daytime Los Angeles anthropogenic emission replica experiment (see Table S4).
[k] Value of toluene from the same experiment.
[M] Observed signal decrease from MR-CIMS (benzene reagent).
[N] Observed signal decrease from NH_4^+-Vocus.

Table S4. List of injected VOCs for experiments using the replicas of Los Angeles city anthropogenic emission, global city anthropogenic emission, and future city anthropogenic+biogenic emission as precursors. The mixing ratio of expected injected VOCs (inj., in ppb), the percentage of consumed VOCs (% cons.), and the mixing ratio of expected consumed VOCs (cons., in ppb) are listed. The percentage of consumed VOCs is based on the concentration decrease or signal decrease of mass from observations (labeled with superscript uppercase letter, see footnote). Compounds with unavailable information of signal decrease use the value or average from other compounds with similar structure and/or other experiments with similar conditions (labeled with superscript lowercase letter, see footnote).

VOC	Formula	Los Angeles anthropogenic emission						global city anthropogenic emission			future city anthr.+biogenic emission		
		daytime medium NO			nighttime			daytime medium NO			daytime low NO		
		inj. (ppb)	% cons.	cons. (ppb)	inj. (ppb)	% cons.	cons. (ppb)	inj. (ppb)	% cons.	cons. (ppb)	inj. (ppb)	% cons.	cons. (ppb)
Aldehydes (saturated and unsaturated)													
acetaldehyde	C_2H_4O	12.05	47 %[a]	5.69	12.05	37 %[N]	4.45	11.96	47 %[a]	5.65	9.96	47 %[a]	4.70
acrolein	C_3H_4O	-	-	-	-	-	-	0.93	20 %[a]	0.18	-	-	-
propanal	C_3H_6O	13.11	91 %[b]	11.97	13.11	91 %[b]	11.97	15.59	91 %[b]	14.24	12.54	91 %[N]	11.45
methacrylaldehyde	C_4H_6O	-	-	-	-	-	-	0.65	20 %[c]	0.13	-	-	-
pentenal	C_5H_8O	3.29	95 %[M]	3.12	3.29	41 %[M]	1.35	2.90	89 %[M]	2.58	3.15	97 %[M]	3.04
hexadienal	C_6H_8O	5.70	96 %[M]	5.48	5.70	56 %[M]	3.20	5.02	89 %[M]	4.44	5.45	90 %[M]	4.89
heptanal	$C_7H_{14}O$	2.45	56 %[b]	1.38	2.45	25 %[N]	0.61	2.15	56 %[b]	1.21	2.34	56 %[N]	1.32
octenal	$C_8H_{14}O$	1.10	81 %[N]	0.90	1.10	46 %[N]	0.50	0.97	68 %[N]	0.66	1.06	80 %[N]	0.85
nonanal	$C_9H_{18}O$	0.96	97 %[N]	0.93	0.96	64 %[N]	0.61	0.85	91 %[N]	0.77	0.92	92 %[N]	0.84
decanal	$C_{10}H_{20}O$	1.31	62 %[b]	0.82	1.31	22 %[N]	0.29	1.15	62 %[b]	0.72	1.25	62 %[N]	0.78
tridecanal	$C_{13}H_{26}O$	0.06	62 %[d]	0.04	0.06	22 %[d]	0.01	0.05	62 %[d]	0.03	0.06	62 %[d]	0.03
Alkanes													
isobutane	C_4H_{10}	17.60	28 %[G]	4.91	17.60	18 %[G]	3.11	11.00	28 %[e]	3.07	16.50	23 %[G]	3.80
2-methylbutane	C_5H_{12}	3.39	29 %[G]	1.00	3.39	22 %[G]	0.74	5.80	29 %[e]	1.71	-	-	-
dodecane	$C_{12}H_{26}$	11.67	67 %[G]	7.77	11.67	31 %[G]	3.62	20.36	67 %[e]	13.55	8.63	62 %[G]	5.35
octadecane	$C_{18}H_{38}$	0.36	67 %[f]	0.24	0.36	31 %[f]	0.11	1.02	67 %[f]	0.68	0.34	62 %[f]	0.21
nonadecane	$C_{19}H_{40}$	-	-	-	-	-	-	0.80	67 %[f]	0.53	-	-	-
eicosane	$C_{20}H_{42}$	-	-	-	-	-	-	0.96	67 %[f]	0.64	-	-	-
heneicosane	$C_{21}H_{44}$	-	-	-	-	-	-	0.53	67 %[f]	0.35	-	-	-
docosane	$C_{22}H_{46}$	-	-	-	-	-	-	0.33	67 %[f]	0.22	-	-	-
Alkenes													
ethylene	C_2H_4	8.60	36 %[G]	3.12	8.60	18 %[G]	1.57	27.00	36 %[e]	9.81	-	-	-
1-propene	C_3H_6	4.40	66 %[G]	2.92	4.40	30 %[G]	1.33	12.50	66 %[e]	8.30	-	-	-
1,3-butadiene	C_4H_6	0.64	100 %[g]	0.64	0.64	100 %[g]	0.64	1.00	100 %[g]	1.00	-	-	-
trans-2-butene	C_4H_8	0.26	83 %[G]	0.22	0.26	87 %[G]	0.23	0.43	83 %[e]	0.36	-	-	-
isobutene	C_4H_8	1.20	71 %[G]	0.85	1.20	47 %[G]	0.57	2.00	71 %[e]	1.42	-	-	-
cyclopentene	C_5H_8	-	-	-	-	-	-	0.22	71 %[h]	0.16	-	-	-
cis-2-pentene	C_5H_{10}	0.16	92 %[G]	0.15	0.16	77 %[G]	0.13	0.28	92 %[e]	0.26	-	-	-
Aromatics													
benzene	C_6H_6	1.07	44 %[i]	0.47	1.07	42 %[i]	0.45	1.83	39 %[i]	0.71	-	-	-
toluene	C_7H_8	5.27	44 %[M]	2.33	5.27	42 %[M]	2.23	4.98	39 %[M]	1.92	3.51	79 %[M]	2.79
o-xylene	C_8H_{10}	0.58	58 %[M]	0.33	0.58	30 %[M]	0.17	0.98	46 %[M]	0.45	-	-	-
m-xylene	C_8H_{10}	5.76	58 %[M]	3.32	5.76	30 %[M]	1.71	4.40	46 %[M]	2.01	4.74	55 %[M]	2.60
p-xylene	C_8H_{10}	0.78	58 %[M]	0.45	0.78	30 %[M]	0.23	1.33	46 %[M]	0.61	-	-	-
1,2,4-trimethylbenzene	C_9H_{12}	0.38	13 %[a]	0.05	0.38	13 %[a]	0.05	0.65	13 %[a]	0.09	-	-	-
1,3,5-trimethylbenzene	C_9H_{12}	-	-	-	-	-	-	1.63	52 %[a]	0.86	-	-	-
Isoprene, terpenes, and terpenoids													
isoprene	C_5H_8	-	-	-	-	-	-	-	-	-	16.46	96 %[M]	15.82
camphene	$C_{10}H_{16}$	-	-	-	-	-	-	-	-	-	0.98	98 %[k]	0.96
limonene	$C_{10}H_{16}$	2.71	98 %[G]	2.66	2.71	100 %[G]	2.71	1.80	98 %[e]	1.76	4.34	100 %[G]	4.33
α-pinene	$C_{10}H_{16}$	0.32	67 %[G]	0.21	0.32	91 %[G]	0.29	0.19	67 %[e]	0.13	5.00	99 %[G]	4.96
β-pinene	$C_{10}H_{16}$	0.32	100 %[G]	0.32	0.32	100 %[G]	0.32	0.19	100 %[e]	0.19	1.08	96 %[G]	1.05
β-myrcene	$C_{10}H_{16}$	-	-	-	-	-	-	-	-	-	0.78	98 %[k]	0.77
eucalyptol	$C_{10}H_{18}O$	-	-	-	-	-	-	-	-	-	0.87	98 %[k]	0.85
α-cedrene	$C_{15}H_{24}$	-	-	-	-	-	-	-	-	-	0.91	98 %[k]	0.90

Continues next page

Table S4. (continued)

VOC	Formula	Los Angeles anthropogenic emission daytime medium NO inj. (ppb)	% cons.	cons. (ppb)	Los Angeles anthropogenic emission nighttime inj. (ppb)	% cons.	cons. (ppb)	global city anthropogenic emission daytime medium NO inj. (ppb)	% cons.	cons. (ppb)	future city anthr.+biogenic emission daytime low NO inj. (ppb)	% cons.	cons. (ppb)
Alcohols, ethers, amines, and others													
ethanol	C_2H_6O	88.79	23 %[b]	20.58	88.79	25 %[N]	22.10	64.43	23 %[b]	14.94	80.44	23 %[N]	18.65
ethylene glycol	$C_2H_6O_2$	3.82	13 %[m]	0.51	3.82	26 %[N]	0.98	2.35	13 %[b]	0.31	3.63	13 %[b]	0.48
ethanolamine	C_2H_7NO	1.36	3 %[m]	0.04	1.36	3 %[m]	0.04	0.84	3 %[m]	0.02	1.29	3 %[m]	0.04
isopropyl alcohol	C_3H_8O	29.20	24 %[b]	7.15	29.20	25 %[N]	7.32	17.99	24 %[b]	4.40	27.76	24 %[N]	6.79
propylene glycol	$C_3H_8O_2$	14.94	20 %[n]	3.00	14.94	26 %[N]	3.84	9.20	20 %[N]	1.85	14.20	57 %[N]	8.03
tetrahydrofuran	C_4H_8O	1.22	37 %[m]	0.45	1.22	26 %[N]	0.32	0.75	37 %[m]	0.28	1.16	37 %[m]	0.43
2-butoxyethanol	$C_6H_{14}O_2$	0.61	28 %[n]	0.17	0.61	26 %[N]	0.16	0.37	28 %[N]	0.10	0.58	50 %[N]	0.29
carbitol	$C_6H_{14}O_3$	0.44	53 %[n]	0.23	0.44	29 %[N]	0.13	0.27	53 %[N]	0.14	0.42	70 %[N]	0.29
triethanolamine	$C_6H_{15}NO_3$	0.25	3 %[p]	0.01	0.25	3 %[p]	0.01	0.16	3 %[p]	0.004	0.24	3 %[p]	0.01
D5-siloxane	$C_{10}H_{30}O_5Si_5$	0.98	17 %[b]	0.17	0.98	26 %[N]	0.25	0.60	17 %[b]	0.10	0.93	17 %[N]	0.16
	Summary	**247.12**	**38 %**	**94.58**	**247.12**	**32 %**	**78.35**	**241.42**	**43 %**	**103.55**	**231.52**	**46 %**	**107.45**

[a] Value or average value of the compound from the daytime diesel/gasoline experiment(s) with available observation (see Table S3).
[b] Value of the compound from the daytime low NO future city anthropogenic+biogenic emission replica experiment.
[c] Value of acrolein from the same experiment.
[d] Value of decanal from the same experiment.
[e] Value of the compound from the daytime medium NO Los Angeles anthropogenic emission replica experiment.
[f] Value of dodecane from the same experiment.
[g] Value or average value of the compound from the daytime Los Angeles anthropogenic+biogenic emission replica experiment(s) with available observation (see Table S5).
[h] Value of isobutene from the daytime medium NO Los Angeles anthropogenic emission replica experiment.
[i] Value of toluene from the same experiment.
[k] Average value of limonene, α-pinene, and β-pinene from the same experiment.
[m] Value or average value of the compound from the daytime VCPs experiment(s) with available observation (see Table S2).
[n] Value of the compound from the daytime medium NO global city anthropogenic emission replica experiment.
[p] Value of ethanolamine from the same experiment.
[G] Observed signal decrease from GC-TD-FID/MS.
[M] Observed signal decrease from MR-CIMS (benzene reagent).
[N] Observed signal decrease from NH_4^+-Vocus.

Table S5. List of injected VOCs for experiments using the replicas of Los Angeles city anthropogenic+biogenic emission as precursors. The mixing ratio of expected injected VOCs (inj., in ppb), the percentage of consumed VOCs (% cons.), and the mixing ratio of expected consumed VOCs (cons., in ppb) are listed. The percentage of consumed VOCs is based on the concentration decrease or signal decrease of mass from observations (labeled with superscript uppercase letter, see footnote). Compounds with unavailable information of signal decrease use the value or average from other compounds with similar structure and/or other experiments with similar conditions (labeled with superscript lowercase letter, see footnote).

VOC	Formula	Los Angeles anthropogenic+biogenic emission											
		daytime low NO			daytime medium NO			daytime high NO			nighttime		
		inj. (ppb)	% cons.	cons. (ppb)	inj. (ppb)	% cons.	cons. (ppb)	inj. (ppb)	% cons.	cons. (ppb)	inj. (ppb)	% cons.	cons. (ppb)
Aldehydes (saturated and unsaturated)													
acetaldehyde	C_2H_4O	10.01	47 %[a]	4.73	10.01	47 %[a]	4.73	10.01	47 %[a]	4.73	10.01	37 %[b]	3.70
propanal	C_3H_6O	10.88	91 %[c]	9.93	10.88	91 %[c]	9.93	10.88	91 %[c]	9.93	10.88	91 %[c]	9.93
pentenal	C_5H_8O	2.73	96 %[M]	2.61	2.73	90 %[M]	2.45	2.73	93 %[d]	2.53	2.73	43 %[M]	1.17
hexadienal	C_6H_8O	4.73	96 %[M]	4.53	4.73	84 %[M]	3.98	4.73	90 %[d]	4.26	4.73	49 %[M]	2.33
heptanal	$C_7H_{14}O$	2.03	57 %[N]	1.16	2.03	48 %[d]	0.97	2.03	38 %[N]	0.78	2.03	25 %[b]	0.51
octenal	$C_8H_{14}O$	0.92	87 %[M]	0.80	0.92	76 %[M]	0.69	0.92	82 %[d]	0.75	0.92	32 %[M]	0.29
nonanal	$C_9H_{18}O$	0.80	95 %[M]	0.76	0.80	89 %[M]	0.71	0.80	92 %[d]	0.74	0.80	59 %[M]	0.47
decanal	$C_{10}H_{20}O$	1.09	69 %[N]	0.75	1.09	58 %[d]	0.63	1.09	47 %[N]	0.51	1.09	22 %[b]	0.24
tridecanal	$C_{13}H_{26}O$	0.05	69 %[e]	0.03	0.05	58 %[e]	0.03	0.05	47 %[e]	0.02	0.05	22 %[e]	0.01
Alkanes													
isobutane	C_4H_{10}	15.40	36 %[G]	5.56	15.40	27 %[d]	4.17	15.40	18 %[G]	2.78	15.40	18 %[b]	2.73
2-methylbutane	C_5H_{12}	2.84	32 %[G]	0.91	2.84	25 %[d]	0.71	2.84	18 %[G]	0.51	2.84	22 %[b]	0.62
dodecane	$C_{12}H_{26}$	9.94	75 %[G]	7.44	9.94	57 %[d]	5.65	9.94	39 %[G]	3.86	9.94	31 %[b]	3.08
octadecane	$C_{18}H_{38}$	0.31	75 %[f]	0.23	0.31	57 %[f]	0.18	0.31	39 %[f]	0.12	0.31	31 %[f]	0.10
Alkenes													
ethylene	C_2H_4	7.30	47 %[G]	3.45	7.30	39 %[d]	2.84	7.30	30 %[G]	2.23	7.30	18 %[b]	1.33
1-propene	C_3H_6	3.70	72 %[G]	2.67	3.70	60 %[d]	2.23	3.70	48 %[G]	1.79	3.70	30 %[b]	1.11
1,3-butadiene	C_4H_6	0.54	100 %[G]	0.54	0.54	100 %[d]	0.54	0.54	100 %[G]	0.54	0.54	100 %[b]	0.54
trans-2-butene	C_4H_8	0.22	95 %[G]	0.21	0.22	98 %[d]	0.21	0.22	100 %[G]	0.22	0.22	87 %[b]	0.19
isobutene	C_4H_8	1.00	88 %[G]	0.88	1.00	76 %[d]	0.76	1.00	64 %[G]	0.64	1.00	47 %[b]	0.47
cis-2-pentene	C_5H_{10}	0.14	90 %[G]	0.12	0.14	89 %[d]	0.12	0.14	89 %[G]	0.12	0.14	77 %[b]	0.11
Aromatics													
benzene	C_6H_6	0.90	75 %[g]	0.68	0.90	64 %[g]	0.58	0.90	70 %[g]	0.63	0.90	42 %[g]	0.38
toluene	C_7H_8	4.48	75 %[M]	3.38	4.48	64 %[M]	2.89	4.48	70 %[d]	3.13	4.48	42 %[b]	1.90
o-xylene	C_8H_{10}	0.48	70 %[M]	0.34	0.48	53 %[M]	0.25	0.48	61 %[d]	0.30	0.48	30 %[b]	0.14
m-xylene	C_8H_{10}	4.92	70 %[M]	3.45	4.92	53 %[M]	2.59	4.92	61 %[d]	3.02	4.92	30 %[b]	1.46
p-xylene	C_8H_{10}	0.65	70 %[M]	0.46	0.65	53 %[M]	0.34	0.65	61 %[d]	0.40	0.65	30 %[b]	0.19
1,2,4-trimethylbenzene	C_9H_{12}	0.32	13 %[a]	0.04	0.32	13 %[a]	0.04	0.32	13 %[a]	0.04	0.32	13 %[a]	0.04
Isoprene, terpenes, and terpenoids													
isoprene	C_5H_8	14.58	98 %[G]	14.34	14.58	96 %[d]	13.94	14.58	93 %[G]	13.53	14.58	61 %[M]	8.95
camphene	$C_{10}H_{16}$	0.87	99 %[h]	0.86	0.87	93 %[h]	0.81	0.87	98 %[h]	0.85	0.87	99 %[h]	0.86
limonene	$C_{10}H_{16}$	3.87	100 %[G]	3.87	3.87	93 %[M]	3.61	3.87	100 %[G]	3.87	3.87	99 %[M]	3.83
α-pinene	$C_{10}H_{16}$	4.44	100 %[G]	4.42	4.44	93 %[M]	4.14	4.44	99 %[G]	4.39	4.44	99 %[M]	4.39
β-pinene	$C_{10}H_{16}$	0.97	98 %[G]	0.94	0.97	93 %[M]	0.90	0.97	94 %[G]	0.91	0.97	99 %[M]	0.95
β-myrcene	$C_{10}H_{16}$	0.69	99 %[h]	0.69	0.69	93 %[h]	0.65	0.69	98 %[h]	0.68	0.69	99 %[h]	0.69
eucalyptol	$C_{10}H_{18}O$	0.77	99 %[h]	0.76	0.77	93 %[h]	0.72	0.77	98 %[h]	0.75	0.77	99 %[h]	0.76
α-cedrene	$C_{15}H_{24}$	0.81	99 %[h]	0.80	0.81	93 %[h]	0.76	0.81	98 %[h]	0.79	0.81	99 %[h]	0.80

Continues next page

Table S5. (continued)

VOC	Formula	Los Angeles anthropogenic+biogenic emission											
		daytime low NO			daytime medium NO			daytime high NO			nighttime		
		inj. (ppb)	% cons.	cons. (ppb)	inj. (ppb)	% cons.	cons. (ppb)	inj. (ppb)	% cons.	cons. (ppb)	inj. (ppb)	% cons.	cons. (ppb)
Alcohols, ethers, amines, and others													
ethanol	C_2H_6O	75.40	23 %[N]	16.99	75.40	23 %[d]	16.99	75.40	23 %[d]	16.99	75.40	23 %[h]	16.99
ethylene glycol	$C_2H_6O_2$	3.27	13 %[i]	0.43	3.27	13 %[i]	0.43	3.27	13 %[i]	0.43	3.27	26 %[b]	0.84
ethanolamine	C_2H_7NO	1.16	3 %[i]	0.03	1.16	3 %[i]	0.03	1.16	3 %[i]	0.03	1.16	3 %[i]	0.03
isopropyl alcohol	C_3H_8O	24.99	26 %[N]	6.40	24.99	26 %[d]	6.40	24.99	26 %[d]	6.40	24.99	26 %[d]	6.40
propylene glycol	$C_3H_8O_2$	12.78	47 %[N]	6.03	12.78	33 %[d]	4.26	12.78	19 %[N]	2.49	12.78	26 %[b]	3.29
tetrahydrofuran	C_4H_8O	1.05	37 %[i]	0.39	1.05	37 %[i]	0.39	1.05	37 %[i]	0.39	1.05	26 %[b]	0.27
2-butoxyethanol	$C_6H_{14}O_2$	0.52	61 %[N]	0.31	0.52	48 %[d]	0.25	0.52	35 %[N]	0.18	0.52	26 %[b]	0.13
carbitol	$C_6H_{14}O_3$	0.38	80 %[N]	0.30	0.38	80 %[d]	0.30	0.38	80 %[d]	0.30	0.38	29 %[b]	0.11
triethanolamine	$C_6H_{15}NO_3$	0.22	3 %[k]	0.01	0.22	3 %[k]	0.01	0.22	3 %[k]	0.01	0.22	3 %[k]	0.01
D5-siloxane	$C_{10}H_{30}O_5Si_5$	0.84	15 %[N]	0.13	0.84	15 %[d]	0.13	0.84	15 %[d]	0.13	0.84	15 %[d]	0.13
	Summary	**233.95**	**48 %**	**113.38**	**233.95**	**44 %**	**102.96**	**233.95**	**42 %**	**97.70**	**233.95**	**35 %**	**82.47**

[a] Value or average value of the compound from the daytime diesel/gasoline experiment(s) with available observation (see Table S3)
[b] Value of the compound from the nighttime Los Angeles anthropogenic emission replica experiment (see Table S4).
[c] Value of the compound from the daytime low NO future city anthropogenic+biogenic emission replica experiment (see Table S4).
[d] Value or average value of the compound from the daytime Los Angeles anthropogenic+biogenic emission replica experiment(s) with available observation.
[e] Value of decanal from the same experiment.
[f] Value of dodecane from the same experiment.
[g] Value of toluene from the same experiment.
[h] Average value of limonene, α-pinene, and β-pinene from the same experiment.
[i] Value or average value of the compound from the daytime VCPs experiment(s) with available observation (see Table S2).
[k] Value of ethanolamine from the same experiment.
[G] Observed signal decrease from GC-TD-FID/MS.
[M] Observed signal decrease from MR-CIMS (benzene reagent).
[N] Observed signal decrease from NH_4^+-Vocus.

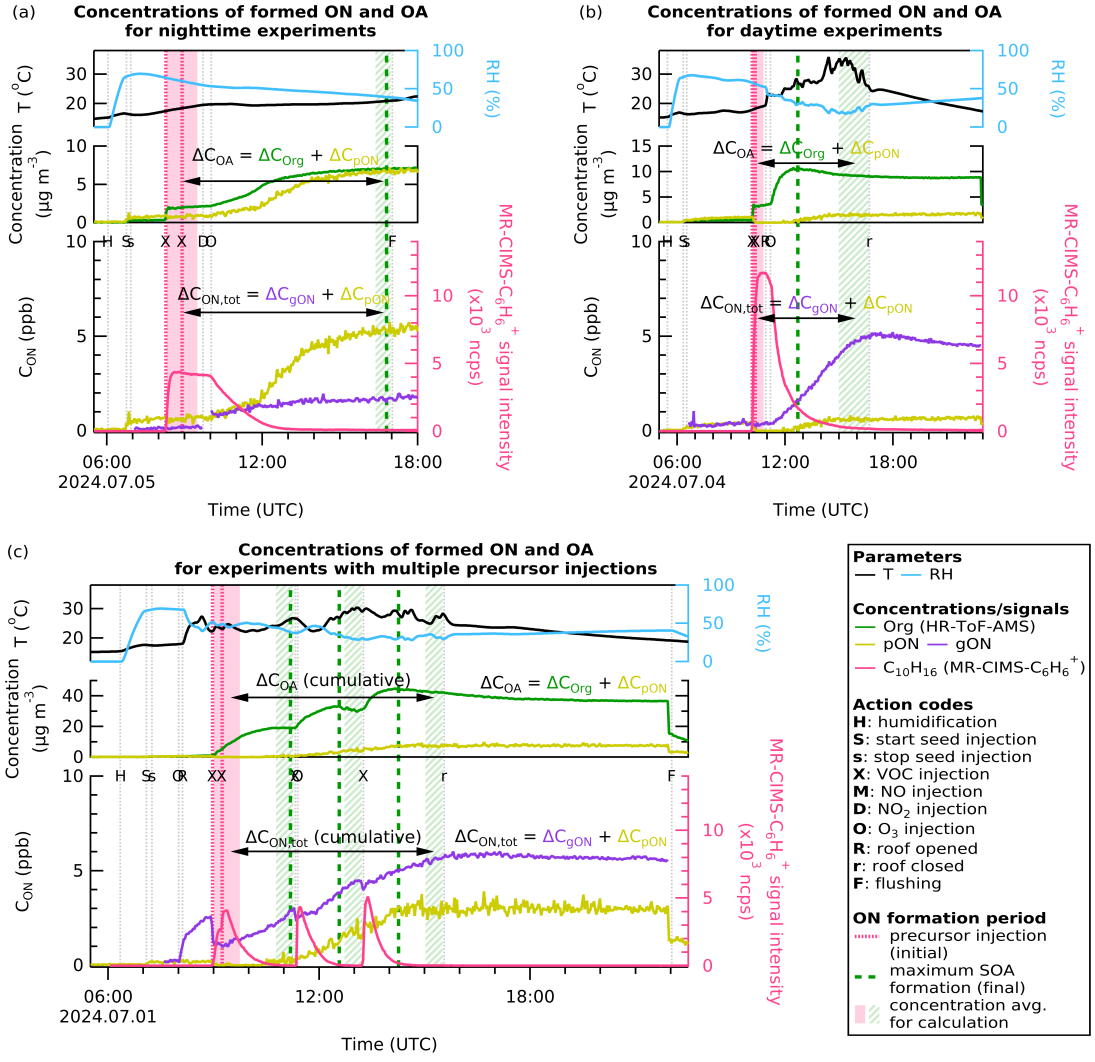

Figure S1. Time series of various chemical species to define initial and final concentrations of formed ON and OA for selected experiments: **(a)** a nighttime experiment with VCP precursors, **(b)** a daytime low NO experiment with VCP precursors, and **(c)** a daytime low NO experiment with limonene added at three different times. The upper left axis shows the temperature in °C and the upper right axis shows the relative humidity (RH) in %. The middle left axis shows the total concentration of organic species (Org) detected by HR-ToF-AMS and pON (as NO_3) in µg m^{-3}. The lower left axis shows the concentrations of gas phase ON (gON) and particle phase ON (pON) in ppb. The concentrations of pON and OA are wall loss and dilution corrected and the concentrations of gON are dilution corrected. The lower right axis shows the signal intensity in ncps of monoterpenes ($C_{10}H_{16}$) detected by MR-CIMS-$C_6H_6^+$. To calculate the particle-to-gas ratio (C_{pON}/C_{gON}) and partitioning coefficient ($K_{p,ON}$), average concentrations of the respective species after SOA formation has peaked are used to represent "equilibrium" conditions (striped green period). For estimating the ON molar yield, the total ON formed ($\Delta C_{ON,tot}$, both gas- and particle-phase) and total OA formed (ΔC_{OA} which includes AMS Org and pON) are calculated by subtracting the "equilibrium" concentrations (striped green period) from the average concentrations following precursor injection(s), which represent the initial condition (red period).

S2 Instrument details

S2.1 NO_x^+ ratio method to separate particulate ammonium nitrate and organic nitrate from HR-ToF-AMS signal

The basis of the method lies in the difference in fragmentation patterns between $RONO_2$ and NH_4NO_3 in the mass spectrometer's vaporizer and ionizer, which results in different NO_2^+/NO^+ ratios. Thus, these compounds can be separated using the variation of NO_2^+/NO^+ ion ratios (which are referred to as NO_x^+ ratios, or R_ν in Eq. S1) from the mass spectra. The NO_x^+ ratio of the observed air in the chamber (R_{obs}) varies between the NO_x^+ ratios of pure particulate ammonium nitrate (R_{pAmN}) and pure particulate organic nitrate (R_{pON}). The time-varying mass fractions of particulate organic nitrate (f_{pON}) can be extracted from R_{obs} using Eq. S2. In Eq. S2, the R_{pAmN} value is obtained from calibrations, while R_{pON} is obtained as $R_{pAmN}/2.75$ according to the empirical parameterization of Day et al. (2022).

$$R_\nu = \frac{(C_{NO_2^+})_\nu}{(C_{NO^+})_\nu} \tag{S1}$$

$$f_{pON} = \frac{(R_{obs} - R_{pAmN})(1 + R_{pON})}{(R_{pON} - R_{pAmN})(1 + R_{obs})} \tag{S2}$$

ν: nitrate compound or mixture measured

$C_{NO_2^+}$: signal intensity of NO_2^+

C_{NO^+}: signal intensity of NO^+

Takeuchi et al. (2024) shows that the vaporization and ionization using a standard vaporizer AMS, results in pON being detected as $-NO_2$ moiety rather than $-ONO_2$. The missing oxygen for the nitrate function group stays attached to the carbon and thus detected as an organic moiety. Thus, pON mass concentration (C_{pON}) calculated from the total pNO_3 mass concentration (C_{pNO_3}) needs to be corrected for this phenomenon using the molar mass ratio of NO_3/NO_2 (62 g mol^{-1}/46 g mol^{-1}) as shown in Eq. S3.

$$C_{pON} = C_{pNO_3} \cdot f_{pON} \cdot \frac{62\ \text{g mol}^{-1}}{46\ \text{g mol}^{-1}} \tag{S3}$$

S2.2 Response of the NO_x analyzer with a modified NO_y inlet to nitrogen-containing species

The response of the NO_x analyzer with a chemiluminescent detector (CLD) and a modified NO_y inlet to inorganic and organic nitrogen species was characterized using co-located measurements from other instruments. The instrument's response to NO_3 and NH_4 was evaluated using aqueous ammonium nitrate and ammonium sulfate solutions and compared with the response of a time-of-flight aerosol chemical speciation monitor (ToF-ACSM). To assess the response to organic nitrate ($RONO_2$ or ON), 2-ethylhexyl nitrate (EHN) in liquid form was used. The CLD response was compared with that of a proton-transfer-reaction time-of-flight mass spectrometer (PTR-ToF-MS).

The setup for NH_4NO_3 and $(NH_4)_2SO_4$ measurements is shown in Fig. S2, based on the calibration setup for NH_4NO_3 in an ACSM instrument. Aqueous solutions were prepared by dissolving either ammonium nitrate (NH_4NO_3, 99 %, Sigma-Aldrich) or ammonium sulfate ($(NH_4)_2SO_4$, 99 %, Sigma-Aldrich) to achieve a 5 mM concentration. Particles were generated from the solutions using an atomizer (Aerosol Generator 3076, TSI), followed by drying with a dryer (TOPAS). These particles were then size-selected using a differential mobility analyzer (DMA 308100, TSI), and passed through an aerosol diluter and mixing tube (316 SS Tube Mixer 1/4-34, Koflo). The sample line, made of Teflon tubing, was split into two lines going to the NO_y converter and ToF-ACSM and were kept as short as possible. In the NO_y converter, nitrogen-containing species were converted to NO using a heated external molybdenum Mo converter at 350 °C and subsequently detected by the chemiluminescent detector of the NO_x analyzer (CLD-42iQTL-NO_x analyzer, Thermo Scientific) as NO. Simultaneously, the ToF-ACSM line directed the sample to the instrument equipped with a capture vaporizer (CV), operating at ∼525 °C. Particle concentrations were targeted in the range of 300–3300 particles cm^{-3}. For each concentration , the NO_y line was first diverted to a condensation particle counter (CPC 3750, TSI) for at least 10 min to quantify the particle number concentration, before being reconnected to the NO_y line for at least 20 min of measurements.

The setup for the $RONO_2$ measurements is shown in Fig. S3. Liquid EHN ($C_8H_{17}NO_3$, 97 %, Sigma-Aldrich) was placed in a capped glass reservoir with inlet and outlet lines. The liquid was pressurized using zero air through the inlet to generate gas-phase EHN, which then flowed through the outlet. The EHN gas concentration was diluted by the sampled flow with room air passing through a HEPA filter, using a needle valve to adjust the dilution factor. The Teflon sample line was split into two lines, going to the NO_y and PTR-MS, both kept as short as possible. The NO_y line operated as in the previous setup. A PTR-ToF 1000 (IONICON Analytik GmbH, Austria) equipped with hexapole ion optics was used, operated at a drift-tube pressure of 2.95 mbar and a field strength (E/N) of 110 Td. Transmission calibration was done using the National Physical Laboratory calibration standard (Worton et al., 2023). The concentration of EHN was determined using

its primary fragment ions, including $C_3H_5^+$ (m/Q 41), $C_3H_7^+$ (m/Q 43), $C_4H_9^+$ (m/Q 57), $C_5H_9^+$ (m/Q 69), $C_5H_{11}^+$ (m/Q 71), $C_8H_{15}^+$ (m/Q 111), $C_8H_{17}O^+$ (m/Q 129) (González-Sánchez et al., 2021).

The linear regressions between the response of the CLD-42iQTL-NO_x analyzer and the CV-UMR-ToF-ACSM (for inorganic species), as well as the PTR-ToF-MS (for organic species), are shown in Fig. S4. The instrument has been shown to detect (104 ± 5) % of expected $RONO_2$, which is comparable to 92 % for peroxyacyl nitrate (PANs) and 103 % for ethyl nitrate ($EtNO_3$) (Winer et al., 1974). Nitro compounds (RNO_2), on the other hand, were reported by Winer et al. (1974) to be poorly detected, with only 6–7 % conversion efficiency. For inorganic species, (94 ± 2) % of expected NH_4NO_3 was detected while $(NH_4)_2SO_4$ was not detected. This suggests that the converter decomposes NO_3^- and not NH_3 or NH_4^+. This result is supported by Baylon et al. (2015) who reported only 0.95 % conversion efficiency of NH_3 at 23 % relative humidity (RH).

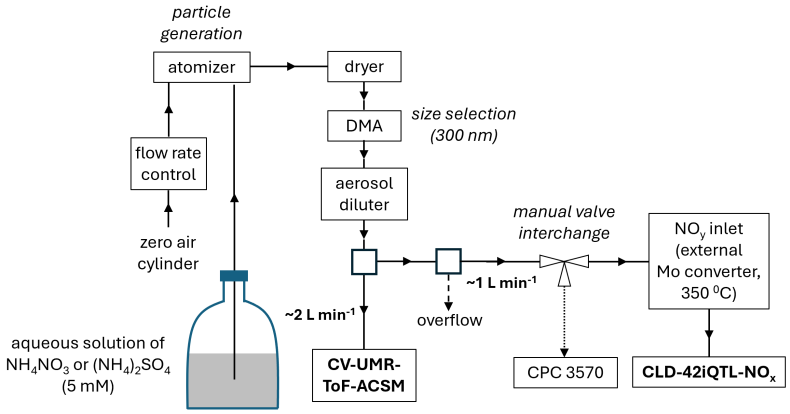

Figure S2. Measurement setup for NH_4NO_3 and $(NH_4)_2SO_4$ using the CLD-42iQTL-NO_x analyzer equipped with NO_y inlet and a CV-UMR-ToF-ACSM.

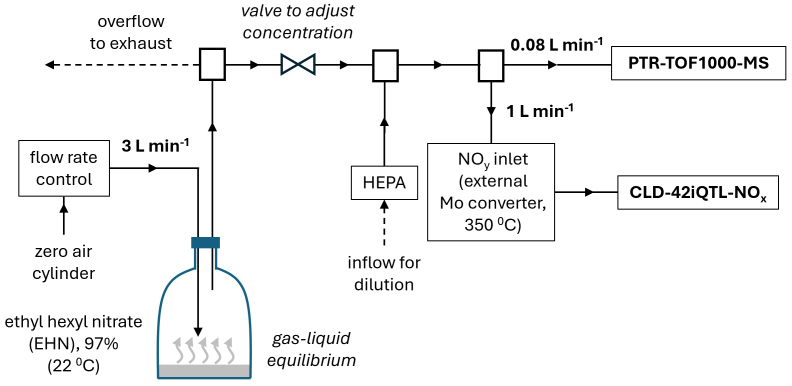

Figure S3. Measurement setup for EHN using the CLD-42iQTL-NO_x analyzer equipped with NO_y inlet and a PTR-ToF1000-MS.

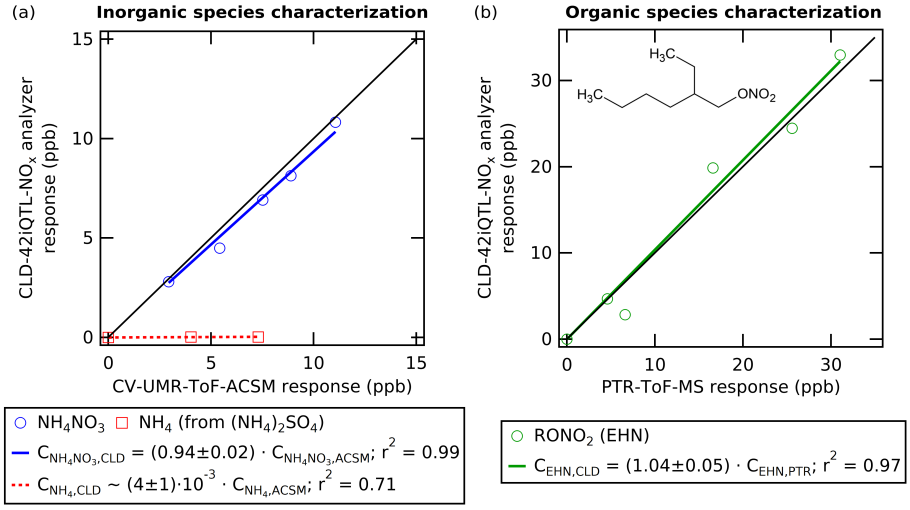

Figure S4. Comparison between the CLD-42iQTL-NO_x analyzer response with an added external NO_y inlet (y-axis) and colocated measurements (x-axis) of NO_z species in ppb. Plot **(a)** shows the comparison for NH_4NO_3 and ($(NH_4)_2SO_4$) between the NO_x analyzer and the CV-UMR-ToF-ACSM, while plot **(b)** shows the comparison for EHN between the NO_x analyzer and the PTR-ToF-MS.

S2.3 Gas phase species measurements using thermal desorption gas chromatography system coupled to dual flame ionization and mass spectrometric detection (GC-TD-FID/MS)

Non-methane hydrocarbons (NMHCs; C_5–C_{12}) were measured with an online thermal desorption (TD) gas chromatography (GC) system coupled to dual flame ionization detector (FID) and mass spectrometry (MS) detection (GC-TD-FID/MS; Markes TT24-7xr with Kori-xr units, Agilent 8890 GC, Agilent 5977B MS). The system targets alkanes, alkenes, alkynes, aromatics, and monoterpenes by cryogenic preconcentration, chromatographic separation, and dual detection (FID for light hydrocarbons, MS for heavier or structurally complex species). The TD unit operated with alternating twin traps, enabling continuous sampling. Each cycle consisted of 44 min sampling at 24 mL min^{-1}, followed by desorption at 300 °C, where helium (6.0 grade) served as carrier gas. GC separation used a three-column setup with a Deans-switch to route lighter compounds to the FID and heavier compounds to the MS. The GC oven program was ramped from 37 °C to 200 °C, with a total runtime of 36 min for each sample. The MS operated in electron impact (EI, 70 eV) full scan mode, with source/interface temperatures of 230 °C, quadrupole at 150 °C, and an emission current of 100 µA. The FID operated at 275 °C with H_2, air, and N_2 makeup flows of 30, 400, and 25 mL min^{-1}, respectively. Due to the alternating traps, the effective time resolution of the system was ~44 min. FID and MS shared identical time resolution as they analyzed the same desorbed sample.

Air from the SAPHIR chamber was drawn through a 7.2 m, 1/4" SilcoNert-coated stainless steel manifold (50 °C), followed by a 1 m, 1/16" SilcoNert-coated line into the instrument. The fully inert-coated sampling path minimized wall losses, especially for unsaturated hydrocarbons. No pre-drying was applied and water was removed downstream in the TD unit. Calibrations were performed with three mixtures: (i) a National Physics Laboratory (NPL) 29-component NMHC standard (C_2–C_8 alkanes, alkenes, aromatics), (ii) an NPL 5-component monoterpene standard, and (iii) a self-prepared multi-compound standard including oxygenates, terpenes, and long-chain alkanes. During the campaign, 20 calibration runs were performed. Blanks using high-purity N_2 and three chamber background measurements were used to assess system background. Limits of detections were determined from calibration runs and varied by compound and trap, typically ranging from 10 to 100 pptv for most hydrocarbons. For instance, ethane, benzene, and isoprene have detection limits of ~60 pptv, ~120 pptv, and ~40 pptv, respectively.

Data acquisition was performed using Agilent ChemStation/OpenLab CDS. FID peaks were semi-automatically integrated and manually inspected. MS analysis was restricted to a fixed target compound list with known retention times and diagnostic ions to improve reproducibility. Concentrations were calculated with Python scripts applying calibration curves consistently. Final datasets were exported with quality assurance including blank subtraction and outlier screening.

S2.4 Gas phase species measurements using multi-reagent chemical-ionization mass spectrometer (MR-CIMS)

The reagent ions of I^- and $C_6H_6^+$ were generated via the charging of methyl iodide (CH_3I) and benzene (C_6H_6), respectively, by two Vacuum Ultra-Violet sources (VUV) (Ji et al., 2020). Equipped with the fast-switch high voltage mode, two VUV sources were switched at a frequency of 1 Hz to generate the positive and negative reagent ion couples. To avoid the variations in RH that have a significant influence on the sensitivity of CIMS (Lee et al., 2014), a dopant flow was directed to introduce water vapor from a heated deionized water bottle to the IMR. The air chamber is sampled at a flow rate $\sim$1.8 SLPM through a 68 cm Teflon tube with an outer diameter of 0.5". The dopant flow rate, whose range was 0 - 30 sccm, was automatically adjusted at a frequency of 0.5 Hz based on the $[H_2OI^-]/[I^-]$ (water ratio) measured in iodide-channel by the TofdaqViewer2 software (Tofwerk AG., Switzerland). The target water ratio was set as 0.6, which was around the maximum ratio measured in the SAPHIR chamber. Due to this dopant flow, the RH in the IMR (kept at 45 °C) was constant throughout the campaign.

The mass resolution ($m/\Delta m$) of the MR-CIMS for cations and anions at m/Q 200 Th are around 5000 and 5300, respectively. The bipolar TOF chamber allows a simultaneous measurement of cations and anions. The data was recorded by a time resolution of 0.5 Hz and consisted of four segments, where each segment corresponds to a different reagent ion. Preliminary analysis of the mass spectrometry data was conducted using the Tofware software package (v4.0.2, Tofwerk AG., Switzerland), including but not limited to data averaging, mass calibration, and peak fitting. The data set was averaged by a factor of two, yielding an effective integration time of 1 s for each reagent ion. Signal intensities of compounds in each detection channel were normalized to 1 million counts per second (ncps) of the corresponding reagent ion signal and then calculated in the unit of ncps. The extraction of time series data was performed using the Tofware software (v4.0.2, Tofwerk AG, Switzerland). Further data processing (i.e., normalization and background subtraction) was carried out using a custom Python v3.7 script. In this work, we obtain the HNO_3 measurements from the iodide channel and VOC species measurements from the benzene channel.

During the campaign, the instrument was calibrated weekly using a 15-compound standard VOC calibration cylinder (ICE-3 FZJ). The sensitivities remained relatively stable, ranging from 10.4 to 13.9 ncps pptv^{-1} for α-pinene, from 6.5 to 8.1 ncps pptv^{-1} for xylene throughout the campaign. The sensitivity of HNO_3 is 9.3 ncps pptv^{-1} and was determined after the campaign with 15 % systematic uncertainty from the calibration. The background was monitored hourly, and no significant variations were observed.

S2.5 Gas phase species measurements using amine-reagent chemical ionization time-of-flight mass spectrometer (amine-ToF)

The amine-ToF applies chemical ionization by using an Eisele type inlet coupled to an atmospheric pressure interface time-of-flight mass spectrometer (CI-APi-ToF-MS) (Eisele and Tanner, 1993; Junninen et al., 2010). The precursor for the primary ion used in this study was propylamine which was prepared as a gas standard before the measurements. Reagent ions were generated by adding the propylamine vapor ($C_3H_7NH_2$, Sigma-Aldrich, purity $\geq$99 %) to the Eisele sheath flow which was irradiated by an americium (^{241}Am) source when introduced into the Eisele inlet, producing $C_3H_7NH_2^+$ ions. After ionizing, the sheath flow entered the drift tube of the Eisele inlet where it was mixed with the sample flow, and the charged primary ions reacted with the analyte molecules.

Two primary reagent ion peaks can be observed in the mass spectrum at mass-to-charge ratios (m/Q) of 60 Th ($C_3H_7NH_2^+$) and 119 Th ($(C_3H_7NH_2)C_3H_7NH_3^+$). The generated $C_3H_7NH_2^+$ reagent ions selectively ionize oxygenated organic compounds by forming adducts with neutral molecules. To reduce the interference of water and suppress possible unwanted reactions in the CI inlet (Berndt, 2021), a dilution flow for the sample air and a sheath flow in the Eisele inlet were introduced. The CI inlet and APi-ToF require a total sample flow of 10.8 L min^{-1}; however, introducing a 10 L min^{-1} of dilution flow in front of the inlet results in only 0.8 L min^{-1} sample flow from the SAPHIR chamber. The sample air passes through a glass tube that transitions from a 14 cm section with a 10 mm inner diameter to another 40 cm section with a 15 mm inner diameter. The flow rate in the first section was 0.8 L min^{-1}, which increases to 10.8 L min^{-1} in the second section after we introduce the dilution flow in between. The residence time of the ions in the ion-molecule-reaction zone is about 200 ms. In this study, the instrument achieved a typical resolving power of 3000–4000 Th/Th. Original data, recorded at 2-second intervals, were averaged at 30-second intervals using the Tofware software package (v3.3.0, Tofwerk AG, Switzerland).

S2.6 Gas phase species measurements using ammonium-reagent Vocus chemical ionization mass spectrometer (NH_4^+-Vocus)

A Vocus long time-of-flight mass spectrometer (Tofwerk AG, Switzerland) operated with ammonium reagent ions (NH_4^+-Vocus) was employed during the campaign to measure VOCs and oxygenated VOCs (OVOCs). The detailed operating principles and instrument setup have been described elsewhere (Krechmer et al., 2018; Xu et al., 2022). The reagent ions, $NH_4^+ \cdot H_2O$, were generated in the ion source by mixing two gas streams, a 21 standard cubic centimeters per minute (sccm) water vapor flow sourced from the headspace of ultra-pure water, and a 0.5 sccm ammonia-containing flow from the headspace of a 0.1 %(v/v) ammonium hydroxide solution. Water molecules were initially

ionized to form H_3O^+, which subsequently reacted with NH_3 to produce NH_4^+ and further clustered with water to form the $NH_4^+ \cdot H_2O$ reagent ions. The Focusing Ion–Molecule Reactor (FIMR) was maintained at 60 °C, 3 mbar, and a drift voltage of 510 V.

VOC sampling was conducted through a heated Teflon tube (2 m in length and 1/4" in outer diameter) with a total flow rate of ~2 SLPM, where 100 sccm of this stream was directed into the FIMR via a 25 mm-long polyetheretherketone (PEEK) capillary with a 0.18 mm inner diameter. Instrument background measurements were conducted for 5 minutes every hour and daily calibrations were conducted using a certified 20-compound VOC gas mixture (NPL Management Ltd., UK). The sensitivity of the instrument remained stable throughout the campaign with 1700 ± 230 cps ppb^{-1} for acetone, 220 ± 30 cps ppb^{-1} for 3-carene, and 4800 ± 600 cps ppb^{-1} for D5-siloxane. Voltage scans for quantification of compounds were conducted at least every hour. The instrument mass resolution was around 9950 Th/Th.

Data were acquired at a time resolution of 1 Hz. Mass calibration, peak fitting, and compound identification were performed using the Tofware software package (v4.0.0, Tofwerk AG, Switzerland). Background subtraction, time averaging, and data cleaning were performed using custom scripts based on the Igor Pro software package.

S2.7 Particle phase measurements using WALL-E coupled to an atmospheric pressure chemical ionization inlet and high-resolution orbitrap mass spectrometer

The Wall-Free Particle Evaporator (WALL-E) interface was developed to thermally desorb aerosol particles while minimizing analyte interaction with instrument surfaces, thereby reducing fragmentation. The system includes a gas-phase denuder, a TD unit with sheath flow, a ceramic spacer for thermal isolation, and a dilution/cooling unit (Gao et al., 2025). WALL-E was coupled to an atmospheric pressure CI inlet (Riva et al., 2019, 2020) connected to a high-resolution Orbitrap mass spectrometer (Q-Exactive, Thermo Fisher Scientific), using bromide ions (Br^-) as reagent ions. Br^- was generated from dibromomethane (Sigma-Aldrich, 99%), continuously supplied at 2 sccm with pure N_2 and ionized via soft X-ray photoionization (Hamamatsu, L9491).

The system was connected to a ~1-liter manifold with 6 SLPM flow rate to reduce residence time and minimize sample losses within the 10 mm stainless steel sampling line. A sample flow of 0.5 SLPM, a hot sheath flow of 0.5 SLPM, and a stable TD temperature of 325 °C were maintained. After desorption, the cooling flow was held constant at 10 SLPM to suppress turbulence at the atmospheric pressure CI inlet (Gao et al., 2025), which was operated by a sheath flow of 24 SLPM and a total flow of 34 SLPM. The Orbitrap was configured with an automatic gain control (AGC) target of $1 \cdot 10^6$ charges, an S-lens RF level of 70, a maximum injection time of 1000 ms, 10 microscans, and a capillary temperature of 150 °C. Mass resolution was set to 140,000 at m/Q 200. Data were analyzed using Orbitool v2.5.2 (Cai et al., 2021), pre-averaged to 1 min intervals. Signals were background-subtracted and normalized to the Br^- signal (m/Q 79). To accurately quantify low-abundance compounds, a linearity correction was applied to all measured signals (Fig. S3 in Riva et al. (2020)).

S3 Uncertainty propagation

S3.1 Uncertainty propagation of ON molar yield

The ON molar yield is calculated by determining the ratio of the mixing ratio of total ON formed in both the gas phase and the particle phase ($\Delta C_{\text{ON,tot}}$) to the mixing ratio of VOC that were consumed ($\Delta C_{\text{VOC,tot}}$). The ON molar yield ($\Delta C_{\text{ON,tot}}/\Delta C_{\text{VOC,tot}}$) is expressed in Eq. S4.

$$\text{ON molar yield} = \frac{\Delta C_{\text{ON,tot}}}{\Delta C_{\text{VOC,tot}}} \cdot 100\% = \frac{(C_{\text{ON,tot}})_f - (C_{\text{ON,tot}})_i}{(C_{\text{VOC,tot}})_f - (C_{\text{VOC,tot}})_i} \cdot 100\% = \frac{(C_{\text{gON}} + C_{\text{pON}})_f - (C_{\text{gON}} + C_{\text{pON}})_i}{(C_{\text{VOC,tot}})_f - (C_{\text{VOC,tot}})_i} \cdot 100\% \quad \text{(S4)}$$

$\Delta C_{\text{ON,tot}}$: mixing ratio of total ON formed in the gas phase and particle phase

$\Delta C_{\text{VOC,tot}}$: mixing ratio of consumed VOCs

$C_{\text{ON,tot}}$: mixing ratio of total ON in the gas phase and particle phase

C_{gON}: mixing ratio of gas phase ON

C_{pON}: mixing ratio of particle phase ON

$C_{\text{VOC,tot}}$: mixing ratio of total VOC

i: initial point (when VOC is added)

f: final point (when maximum SOA concentration is reached)

Therefore, the uncertainty for ON molar yield is propagated from the uncertainties of gas phase ON (gON), particle phase (pON), and VOC mixing ratios at the initial point and final point. The mixing ratio of gON is obtained from Eq. S5, which contains measurements of total NO_y, NO_x, HONO, HNO_3, and pNO_3. Thus, the uncertainty of gON ($\sigma_{C_{\text{gON}}}$) is propagated using Eq. S6 from the uncertainties of

total NO_y ($\sigma_{C_{NO_y}}$ = ±25 ppt), NO_x ($\sigma_{C_{NO_x}}$ = ±40 ppt), HONO ($\sigma_{C_{HONO}}$ = ±40 ppt), HNO_3 ($\sigma_{C_{HNO_3}}$ = ±15 % from MR-CIMS), and pNO_3 ($\sigma_{C_{pNO_3}}$ = ±20 % from AMS).

$$C_{gON} = C_{NO_y} - (C_{NO_x} + C_{HONO} + C_{HNO_3} + C_{pNO_3}) \tag{S5}$$

$$\sigma_{C_{gON}} = \sqrt{\sigma^2_{C_{NO_y}} + \sigma^2_{C_{NO_x}} + \sigma^2_{C_{HONO}} + \sigma^2_{C_{HNO_3}} + \sigma^2_{C_{pNO_3}}} \tag{S6}$$

The mixing ratio of pON is obtained from Eq. S3. Thus, the uncertainty of pON ($\sigma_{C_{pON}}$) is propagated following Eq. S7 from the uncertainties of f_{pON} ($\sigma_{f_{pON}}$ = ±23 %, from NO_x^+ ratio method as described in Takeuchi et al. (2024)) and pNO_3 ($\sigma_{C_{pNO_3}}$ = ±20 % from AMS).

$$\sigma_{C_{pON}} = C_{pON} \cdot \sqrt{\left(\frac{\sigma_{f_{pON}}}{f_{pON}}\right)^2 + \left(\frac{\sigma_{C_{pNO_3}}}{C_{pNO_3}}\right)^2} \tag{S7}$$

Furthermore, we propagate these uncertainties to determine the uncertainty of the mixing ratio of total ON formed ($\sigma_{\Delta C_{ON,tot}}$) using Eq. S8. Similarly, the uncertainty of the mixing ratio of consumed VOCs ($\sigma_{\Delta C_{VOC,tot}}$) is calculated using Eq. S9 from the uncertainty of VOC measurements. Although the signal decrease from various measurements were used, the systematic uncertainty from MR-CIMS signal measurements ($\sigma_{C_{VOC,tot}}$ = ±15 %) is chosen to be the maximum uncertainty in the determining the VOC concentration (assuming other instruments have similar or lower uncertainties). Lastly, the uncertainties are further propagated to obtain the final uncertainty of ON molar yield ($\sigma_{\Delta C_{ON,tot}/\Delta C_{VOC,tot}}$) using Eq. S10.

$$\sigma_{\Delta C_{ON,tot}} = \sqrt{\sigma^2_{C_{gON,i}} + \sigma^2_{C_{pON,i}} + \sigma^2_{C_{gON,f}} + \sigma^2_{C_{pON,f}}} \tag{S8}$$

$$\sigma_{\Delta C_{ON,tot}} = \sqrt{\sigma^2_{C_{VOC,tot,i}} + \sigma^2_{C_{VOC,f}}} \tag{S9}$$

$$\sigma_{\Delta C_{ON,tot}/\Delta C_{VOC,tot}} = \Delta C_{ON,tot}/\Delta C_{VOC,tot} \cdot \sqrt{\left(\frac{\sigma_{\Delta C_{ON,tot}}}{\Delta C_{ON,tot}}\right)^2 + \left(\frac{\sigma_{\Delta C_{VOC,tot}}}{\Delta C_{VOC,tot}}\right)^2} \tag{S10}$$

S3.2 Uncertainty propagation of $pRONO_2$ mass fraction

The $pRONO_2$ mass fraction to the total concentration of formed OA is determined by calculating the ratio of $pRONO_2$ mass concentration formed (ΔC_{pRONO_2}) to the mass concentration of OA formed (ΔC_{OA}). The $pRONO_2$ mass fraction to the total OA ($\Delta C_{pRONO_2}/\Delta C_{OA}$) is expressed in Eqs. S11 and S12.

$$pRONO_2 \text{ mass fraction } (\%) = \frac{\Delta C_{pRONO_2}}{\Delta C_{OA}} \cdot 100\% = \frac{(C_{pRONO_2})_f - (C_{pRONO_2})_i}{(C_{OA})_f - (C_{OA})_i} \cdot 100\% \tag{S11}$$

$$pRONO_2 \text{ mass fraction } (\%) = \frac{\left(C_{pON} \cdot \frac{MW_{pRONO_2}}{62\ g \cdot mol^{-1}}\right)_f - \left(C_{pON} \cdot \frac{MW_{pRONO_2}}{62\ g \cdot mol^{-1}}\right)_i}{\left(C_{Org} + C_{pON} \cdot \frac{46\ g \cdot mol^{-1}}{62\ g \cdot mol^{-1}}\right)_f - \left(C_{Org} + C_{pON} \cdot \frac{46\ g \cdot mol^{-1}}{62\ g \cdot mol^{-1}}\right)_i} \tag{S12}$$

ΔC_{pRONO_2}: total concentration of formed pON as $RONO_2$ (μg m^{-3})

ΔC_{OA}: total concentration of formed Org and pON as $-NO_2$ (μg m^{-3})

C_{pRONO_2}: total concentration of pON as $RONO_2$ (μg m^{-3})

C_{OA}: total concentration of organic aerosol (μg m^{-3})

MW_{pRONO_2}: molecular weight of bulk pON (g mol^{-1})

C_{Org}: total concentration of Org species in AMS (μg m^{-3})

C_{pON}: concentration of pON as $-ONO_2$ in AMS (μg m^{-3})

i: initial point (when VOC is added)

f: final point (when maximum SOA concentration is reached)

Therefore, the uncertainty for $\mathrm{pRONO_2}$ mass fraction is propagated from the uncertainties of pON ($\sigma_{C_{\mathrm{pON}}}$, see Eq. S7), molecular weight of bulk pON ($\sigma_{\mathrm{MW_{pRONO_2}}}$ = ±50 % from WALL-E), and Org ($\sigma_{C_{\mathrm{Org}}}$ = ±20 % from AMS) at the initial point and final point. The uncertainty of $\mathrm{pRONO_2}$ mass concentration ($\sigma_{C_{\mathrm{pRONO_2}}}$) is propagated using Eq. S13 from $\sigma_{C_{\mathrm{pON}}}$ and $\sigma_{\mathrm{MW_{pRONO_2}}}$, which then used to calculate the uncertainty of total $\mathrm{pRONO_2}$ formed ($\sigma_{\Delta C_{\mathrm{pRONO_2}}}$) in Eq. S14. As the molecular weight changes with time due to chemical transformation, the initial molecular weight after the VOC injection and the final molecular weight the SOA concentration is maximum need to be taken into account to correctly calculate the amount of $\mathrm{pRONO_2}$ formed.

$$\sigma_{C_{\mathrm{pRONO_2}}} = C_{\mathrm{pRONO_2}} \cdot \sqrt{\left(\frac{\sigma_{C_{\mathrm{pON}}}}{C_{\mathrm{pON}}}\right)^2 + \left(\frac{\sigma_{\mathrm{MW_{pRONO_2}}}}{\mathrm{MW_{pRONO_2}}}\right)^2} \tag{S13}$$

$$\sigma_{\Delta C_{\mathrm{pRONO_2}}} = \sqrt{\sigma^2_{C_{\mathrm{pRONO_2},i}} + \sigma^2_{C_{\mathrm{pRONO_2},f}}} \tag{S14}$$

The uncertainty of total OA ($\sigma_{\Delta C_{\mathrm{OA}}}$) is propagated using Eq. S15 from $\sigma_{C_{\mathrm{Org}}}$ and $\sigma_{C_{\mathrm{pON}}}$.

$$\sigma_{\Delta C_{\mathrm{OA}}} = \sqrt{\sigma^2_{C_{\mathrm{Org},i}} + \sigma^2_{C_{\mathrm{pON},i}} + \sigma^2_{C_{\mathrm{Org},f}} + \sigma^2_{C_{\mathrm{pON},f}}} \tag{S15}$$

Lastly, the final uncertainty for $\mathrm{pRONO_2}$ mass fraction is obtained by propagating $\sigma_{\Delta C_{\mathrm{pRONO_2}}}$ and $\sigma_{\Delta C_{\mathrm{OA}}}$ using Eq. S16.

$$\sigma_{\Delta C_{\mathrm{pRONO_2}}/\Delta C_{\mathrm{OA}}} = \Delta C_{\mathrm{pRONO_2}}/\Delta C_{\mathrm{OA}} * \cdot \sqrt{\left(\frac{\sigma_{\Delta C_{\mathrm{pRONO_2}}}}{\Delta C_{\mathrm{pRONO_2}}}\right)^2 + \left(\frac{\sigma_{\Delta C_{\mathrm{OA}}}}{\Delta C_{\mathrm{OA}}}\right)^2} \tag{S16}$$

S3.3 Uncertainty propagation of gas-particle partitioning

The effective saturation concentration of organic nitrate (C^*_{ON}, in μg $\mathrm{m^{-3}}$) is calculated using the total mass concentration of the particle phase (m_{tot}, in μg $\mathrm{m^{-3}}$) and the mixing ratios of gON and pON, as shown in Eq. S17. Therefore, the final uncertainty of C^*_{ON} ($\sigma_{C^*_{\mathrm{ON}}}$) is propagated using Eq. S18 from the uncertainties of m_{tot} ($\sigma_{C_{m_{\mathrm{tot}}}}$, ±20 % from AMS), gON ($\sigma_{C_{\mathrm{gON}}}$, see Eq. S6), and pON ($\sigma_{C_{\mathrm{pON}}}$, see Eq. S7). When expressed as $\log(\mathrm{C^*_{ON}})$, the uncertainty calculation follows Eq. S19.

$$C^*_{\mathrm{ON}} = \frac{C_{\mathrm{gON}}}{C_{\mathrm{pON}}} \cdot m_{\mathrm{tot}} \tag{S17}$$

$$\sigma_{C^*_{\mathrm{ON}}} = C^*_{\mathrm{ON}} \cdot \sqrt{\left(\frac{\sigma_{C_{\mathrm{gON}}}}{C_{\mathrm{gON}}}\right)^2 + \left(\frac{\sigma_{C_{\mathrm{pON}}}}{C_{\mathrm{pON}}}\right)^2 + \left(\frac{\sigma_{m_{\mathrm{tot}}}}{m_{\mathrm{tot}}}\right)^2} \tag{S18}$$

$$\sigma_{\log(C^*_{\mathrm{ON}})} = \frac{\sigma_{C^*_{\mathrm{ON}}}}{\ln(10) \cdot C^*_{\mathrm{ON}}} \tag{S19}$$

The gas-particle partitioning coefficient of organic nitrate ($K_{\mathrm{p,ON}}$, in $\mathrm{m^3}$ $\mathrm{\mu g^{-1}}$) is calculated using the mixing ratios of pON and gON, and the total mass concentration of the particle phase (m_{tot}, in μg $\mathrm{m^{-3}}$), as shown in Eq. S20. Therefore, the final uncertainty of $K_{\mathrm{p,ON}}$ ($\sigma_{K_{\mathrm{p,ON}}}$) is propagated using Eq. S21 from the uncertainties of pON ($\sigma_{C_{\mathrm{pON}}}$, see Eq. S7), gON ($\sigma_{C_{\mathrm{gON}}}$, see Eq. S6), and m_{tot} ($\sigma_{C_{m_{\mathrm{tot}}}}$, ±20 % from AMS).

$$K_{\mathrm{p,ON}} = \frac{C_{\mathrm{pON}}}{C_{\mathrm{gON}}} \cdot \frac{1}{m_{\mathrm{tot}}} \tag{S20}$$

$$\sigma_{K_{\mathrm{p,ON}}} = K_{\mathrm{p,ON}} \cdot \sqrt{\left(\frac{\sigma_{C_{\mathrm{pON}}}}{C_{\mathrm{pON}}}\right)^2 + \left(\frac{\sigma_{C_{\mathrm{gON}}}}{C_{\mathrm{gON}}}\right)^2 + \left(\frac{\sigma_{m_{\mathrm{tot}}}}{m_{\mathrm{tot}}}\right)^2} \tag{S21}$$

S4 Summary tables and figures

Table S6. Summary of species mixing ratios/concentrations in the gas-phase and particle-phase during the chamber experiments, expressed in ppb and μg m^{-3}, including nitrogen species (gas phase and particle phase), ozone (O_3), Org, and total particle mass (m_{tot}). All species are not wall loss and dilution corrected.

Experiment	NO condition[a]		Mixing ratio (ppb)[b]								Particle concentration (μg m^{-3})[b]			
	NO (ppb)	NO_2 (ppb)	NO_x	NO_y	HONO	HNO_3	pNO_3	gON[c]	pON[d]	O_3	Total (m_{tot})	Org	pNO_3	pON[d]
Limonene, daytime low NO														
1st limonene inject.	0.19	2.16	2.47	5.96	0.74	0.29	0.21	2.25	0.02	66.50	26.35	17.21	0.52	0.05
2nd limonene inject.			3.03	8.32	0.60	0.50	0.28	3.91	0.14	78.22	32.60	25.65	0.69	0.35
3rd limonene inject.			3.10	9.29	0.59	0.45	0.36	4.79	0.22	81.24	37.67	31.79	0.90	0.54
Limonene, nighttime														
1st limonene inject.	0.00	11.09	13.45	14.90	0.04	0.25	0.07	1.09	0.07	6.91	8.24	1.81	0.17	0.17
2nd limonene inject.			10.62	13.03	0.08	0.42	0.14	1.77	0.14	13.77	11.53	7.31	0.35	0.35
3rd limonene inject.			7.97	10.54	0.11	0.44	0.17	1.85	0.17	7.87	11.05	8.22	0.44	0.44
VCPs														
daytime low NO	0.16	2.21	2.96	8.01	0.35	0.42	0.09	4.19	0.03	114.78	10.83	6.25	0.22	0.08
daytime med. NO	0.27	1.80	2.90	7.30	0.33	0.57	0.06	3.43	0.03	52.19	10.20	4.66	0.16	0.07
daytime high NO	1.00	4.29	4.87	12.78	0.49	2.55	0.07	4.80	0.04	81.08	11.29	4.97	0.17	0.09
nighttime	0.00	10.15	10.72	12.89	0.27	0.26	0.31	1.32	0.18	12.45	12.47	4.92	0.78	0.46
Traffic: Diesel emission														
daytime med. NO	0.31	1.18	1.94	4.25	0.26	0.27	0.03	1.75	0.03	23.84	8.34	1.02	0.07	0.07
daytime high NO	1.05	2.82	3.02	6.86	0.14	0.62	0.06	3.01	0.05	62.12	10.04	2.42	0.15	0.12
Traffic: Gasoline emission														
daytime med. NO	0.27	1.63	2.33	7.42	0.25	0.86	0.03	3.96	0.03	56.22	7.42	1.01	0.07	0.07
daytime high NO	0.92	3.30	3.59	9.84	0.34	1.39	0.05	4.47	0.04	69.22	8.30	1.54	0.11	0.10
Cooking emission														
daytime low NO	0.07	1.03	1.61	5.26	0.35	0.18	0.04	3.08	0.03	106.69	9.86	2.13	0.09	0.06
daytime med. NO	0.24	1.34	2.34	6.36	0.23	0.64	0.03	3.11	0.03	51.53	9.38	1.57	0.08	0.08
Complex urban mixtures: Los Angeles anthropogenic emission														
daytime med. NO	0.22	1.33	2.04	6.45	0.29	0.22	0.04	3.87	0.03	51.47	9.36	3.12	0.11	0.07
nighttime	0.00	12.15	8.54	11.50	0.24	0.22	0.13	2.38	0.09	9.25	9.75	3.53	0.32	0.22
Complex urban mixtures: Los Angeles anthropogenic+biogenic emission														
daytime low NO	0.11	1.52	2.08	6.33	0.23	0.40	0.05	3.58	0.05	77.39	12.63	5.84	0.13	0.12
daytime med. NO	0.15	1.08	1.52	5.40	0.25	0.96	0.05	2.61	0.05	48.89	12.10	6.21	0.13	0.13
daytime high NO	0.23	2.86	2.86	9.05	0.33	0.45	0.10	5.30	0.08	104.74	19.72	9.95	0.25	0.19
nighttime, 1st NO_2+O_3 inject.	0.00	16.93	12.88	16.31	0.34	0.14	0.11	2.84	0.08	13.21	14.62	7.54	0.27	0.21
nighttime, 2nd NO_2+O_3 inject.			13.25	19.60	0.52	0.16	0.26	5.51	0.23	11.74	11.91	7.49	0.66	0.58
Complex urban mixtures: global city and future city emissions														
global city anthropogenic, daytime med. NO	0.18	1.65	2.24	7.16	0.31	0.10	0.03	4.47	0.03	57.64	9.18	1.77	0.08	0.08
future city anthropogenic+biogenic, daytime low NO	0.13	1.47	2.25	7.39	0.37	0.71	0.08	3.98	0.07	67.97	16.81	10.09	0.20	0.17

[a] Average mixing ratios after the chamber's roof was opened until it was closed (daytime experiments), or after NO_2+O_3 injection until flushing (nighttime experiments).

[b] Concentrations or mixing ratios are reported after SOA formation peaked, as shown in Fig. S1. For the 1st and 2nd injections of limonene in the limonene experiments, concentrations or mixing ratios are reported before the next injection of limonene. For the 1st injection of NO_2+O_3 in the experiment of Los Angeles anthropogenic+biogenic emission replica under nighttime conditions, concentrations or mixing ratios are reported before the next injection of NO_2+O_3.

[c] $C_{gON} = C_{NO_y} - C_{NO_x} - C_{HONO} - C_{HNO_3} - C_{pNO_3}$

[d] Obtained using NO_x^+ ratio method to AMS pNO_3, reported as $-ONO_2$.

Table S7. Summary of species mixing ratios/concentrations in the gas-phase (dilution corrected) and particle-phase (wall loss and dilution corrected) during the chamber experiments, expressed in ppb and μg m^{-3}. They include the nitrogen species (gas phase and particle phase), Org, and m_{tot}. The corrected concentrations are used for molar yield and mass fraction calculations in Table 2. The particle-to-gas ratio of ON (C_{pON}/C_{gON}) and gas-particle partitioning coefficient of ON ($K_{p,ON}$) are calculated using two sets of concentrations: the instantaneous measured concentrations (in Table S6), and the wall loss and/or dilution corrected concentrations (this table). Both calculations show similar order of magnitude on the C_{pON}/C_{gON} values (increase of 0.001–0.021 when wall loss/dilution corrected) and $K_{p,ON}$ (no change or decrease up to $3 \cdot 10^{-3}$ m^3 μg^{-1} when wall loss/dilution corrected). The instantaneous measured concentrations and partitioning (uncorrected) are the one showed in the main article to represent the actual partitioning equilibrium in the chamber. Average temperatures at equilibrium ($T_{eq,avg}$, in °C) and relative humidities at equilibrium ($RH_{eq,avg}$, in %) are also listed.

Experiment	Mixing ratio (ppb)[a]			Particle concentration (μg m^{-3})[a]				C_{pON}/C_{gON}[a,e]		$K_{p,ON}$ (m^3 μg^{-1})[a,d,e]		$T_{eq,avg}$[a] (°C)	$RH_{eq,avg}$[a] (%)
	pNO_3[f]	gON[b,g]	pON[c,f]	Total (m_{tot})[f]	Org[f]	pNO_3[f]	pON[c,f]	uncorrected	corrected	uncorrected	corrected		
Limonene, daytime low NO													
1st limonene inject.	0.24	2.38	0.02	30.54	19.06	0.59	0.05	0.008	0.009	3.18E-04	2.94E-04	23.6	42
2nd limonene inject.	0.35	4.21	0.17	41.56	31.02	0.86	0.43	0.035	0.041	1.09E-03	9.87E-04	26.3	30
3rd limonene inject.	0.49	5.36	0.29	53.12	42.57	1.22	0.73	0.045	0.054	1.20E-03	1.03E-03	24.9	33
Limonene, nighttime													
1st limonene inject.	0.08	1.24	0.08	10.85	2.11	0.20	0.20	0.061	0.064	7.37E-03	5.88E-03	17.7	26
2nd limonene inject.	0.18	2.07	0.18	17.12	9.02	0.46	0.46	0.078	0.087	6.79E-03	5.08E-03	19.9	21
3rd limonene inject.	0.28	2.42	0.28	21.36	13.29	0.71	0.71	0.094	0.116	8.55E-03	5.42E-03	18.9	18
VCPs													
daytime low NO	0.16	4.56	0.06	18.74	9.23	0.40	0.15	0.008	0.013	7.25E-04	7.00E-04	27.3	22
daytime med. NO	0.13	3.81	0.06	17.16	7.10	0.31	0.14	0.009	0.015	8.38E-04	8.86E-04	28.5	20
daytime high NO	0.11	5.25	0.05	15.17	6.15	0.25	0.13	0.008	0.010	6.93E-04	6.92E-04	38.8	20
nighttime	0.42	1.56	0.25	19.74	6.78	1.05	0.62	0.138	0.158	1.11E-02	7.99E-03	22.6	43
Traffic: diesel emission													
daytime med. NO	0.05	1.92	0.05	13.49	1.37	0.13	0.12	0.015	0.025	1.84E-03	1.87E-03	29.7	24
daytime high NO	0.09	3.38	0.07	16.28	3.04	0.22	0.17	0.016	0.021	1.60E-03	1.29E-03	34.1	15
Traffic: gasoline emission													
daytime med. NO	0.05	4.56	0.05	12.50	1.34	0.13	0.13	0.007	0.012	1.01E-03	9.25E-04	32.8	18
daytime high NO	0.07	5.05	0.07	13.29	1.96	0.18	0.16	0.009	0.013	1.13E-03	9.84E-04	33.3	19
Cooking emission													
daytime low NO	0.06	3.23	0.04	14.09	2.64	0.15	0.10	0.008	0.013	8.44E-04	8.88E-04	28.2	31
daytime med. NO	0.06	3.46	0.06	15.15	2.20	0.14	0.13	0.011	0.016	1.14E-03	1.05E-03	34.3	15
Complex urban mixtures: Los Angeles anthropogenic emission													
daytime med. NO	0.08	4.44	0.05	15.30	4.44	0.19	0.13	0.008	0.012	8.39E-04	7.86E-04	31.5	19
nighttime	0.21	3.07	0.14	18.75	6.23	0.53	0.36	0.037	0.046	3.81E-03	2.48E-03	26.4	31
Complex urban mixtures: Los Angeles anthropogenic+biogenic emission													
daytime low NO	0.10	4.34	0.09	24.43	10.22	0.25	0.22	0.013	0.021	1.05E-03	8.66E-04	31.9	18
daytime med. NO	0.09	3.00	0.09	20.21	8.72	0.22	0.21	0.020	0.029	1.66E-03	1.45E-03	34.5	13
daytime high NO	0.15	6.14	0.12	29.46	13.75	0.37	0.29	0.015	0.019	7.50E-04	6.58E-04	36.8	18
nighttime, 1st $NO_2 + O_3$ inject.	0.13	3.38	0.11	19.77	8.83	0.34	0.27	0.030	0.032	2.08E-03	1.60E-03	24.2	51
nighttime, 2nd $NO_2 + O_3$ inject.	0.46	7.60	0.40	26.77	14.81	1.15	1.02	0.042	0.054	3.56E-03	2.00E-03	23.9	34

Continues next page

250 **Table S7.** (continued)

Experiment	Mixing ratio (ppb)[a]			Particle concentration (μg m^{-3})[a]				C_{pON}/C_{gON}[a,e]		$K_{p,ON}$ (m^3 μg^{-1})[a,d,e]		$T_{eq,avg}$[a] (°C)	$RH_{eq,avg}$[a] (%)
	pNO_3[f]	gON[b,g]	pON[c,f]	Total (m_{tot})[f]	Org[f]	pNO_3[f]	pON[c,f]	uncorrected	corrected	uncorrected	corrected		
Complex urban mixtures: global city and future city emissions													
global city anthropogenic emission, daytime med. NO	0.06	5.09	0.06	15.25	2.55	0.14	0.14	0.007	0.011	7.75E-04	7.49E-04	39.7	15
future city anthropogenic+biogenic emission, daytime low NO	0.12	4.61	0.10	25.44	13.74	0.29	0.25	0.018	0.022	1.05E-03	8.70E-04	34.3	17

[a] Concentrations/mixing ratios/conditions are reported after SOA formation peaked or before a new precursor injection, as shown in Fig. S1.
[b] $C_{gON} = C_{NO_y} - C_{NO_x} - C_{HONO} - C_{HNO_3} - C_{pNO_3}$ (calculated as uncorrected from loss, then the final C_{gON} is dilution corrected).
[c] Obtained using NO_x^+ ratio method to AMS pNO_3.
[d] $K_{p,ON} = (C_{pON}/C_{gON}) \cdot 1/m_{tot}$
[e] At $T_{eq,avg}$ and $RH_{eq,avg}$.
[f] Wall loss and dilution corrected using the equation $C_t = 9.01 \cdot exp((1.22 \cdot 10^{-4}) \cdot t)$ based on observed $(NH_4)_2SO_4$ decay.
[g] Dilution corrected with a dilution rate varying from $4 \cdot 10^{-4}$ min^{-1} to $6 \cdot 10^{-4}$ min^{-1}.

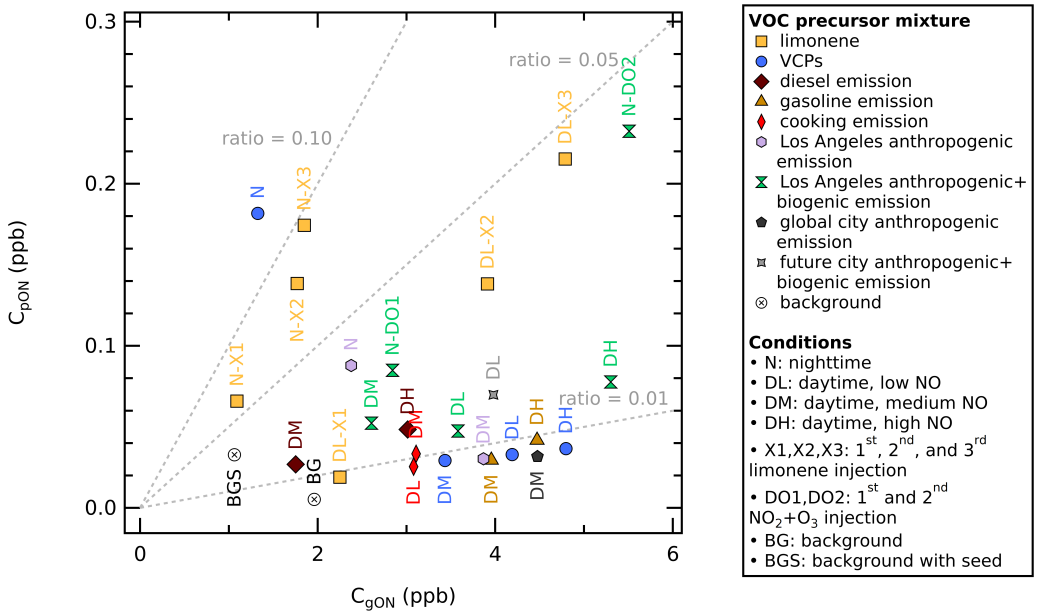

Figure S5. Scatter plot of particle-phase ON (y-axis) vs gas-phase ON (x-axis) mixing ratio in ppb from different VOC-NO_x mixtures, color-coded by VOC precursor mixture. The total absorptive mass of each experiment at equilibrium varies from 13 to 38 μg m^{-3}. The concentrations are the averages under equilibrium conditions. The dotted lines visualize different C_{pON}/C_{gON} values (0.01, 0.05, and 0.10).

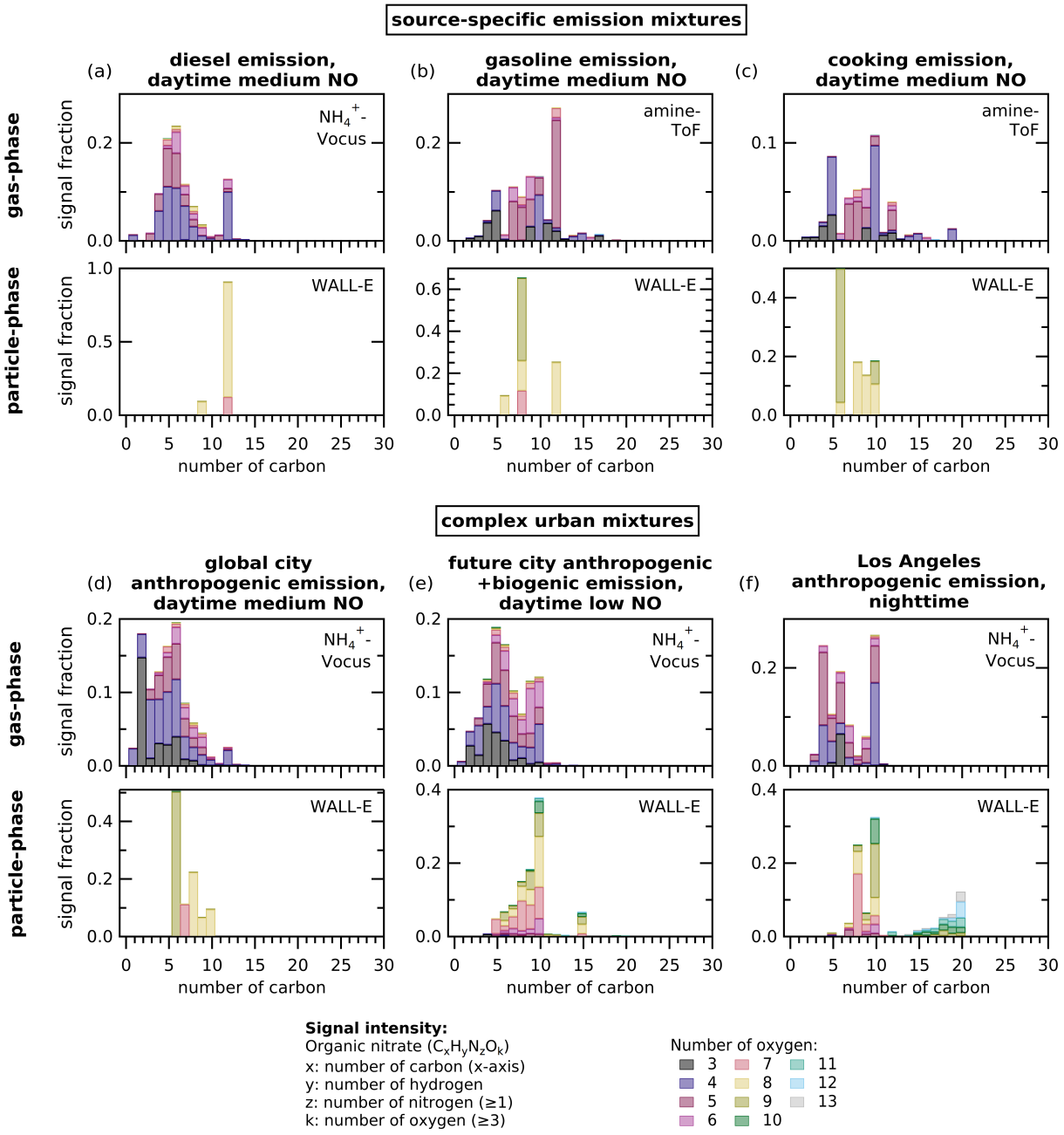

Figure S6. (a-e) The ON composition profiles in the gas phase and particle phase for selected chamber experiments from source-specific emission mixtures and complex urban mixtures at equilibrium. The profiles show the signal fraction from the total signal intensity of detected species from amine-ToF or NH_4^+-Vocus measurements in the gas phase and WALL-E measurements in the particle phase (y-axis) as function of the number of carbon (x-axis). The plots only include compounds with at least one nitrogen atom and three oxygen atoms. The color of the bars represents the signal fraction of compounds with a given number of oxygen atoms for each carbon number, to all considered species in individual experiment.

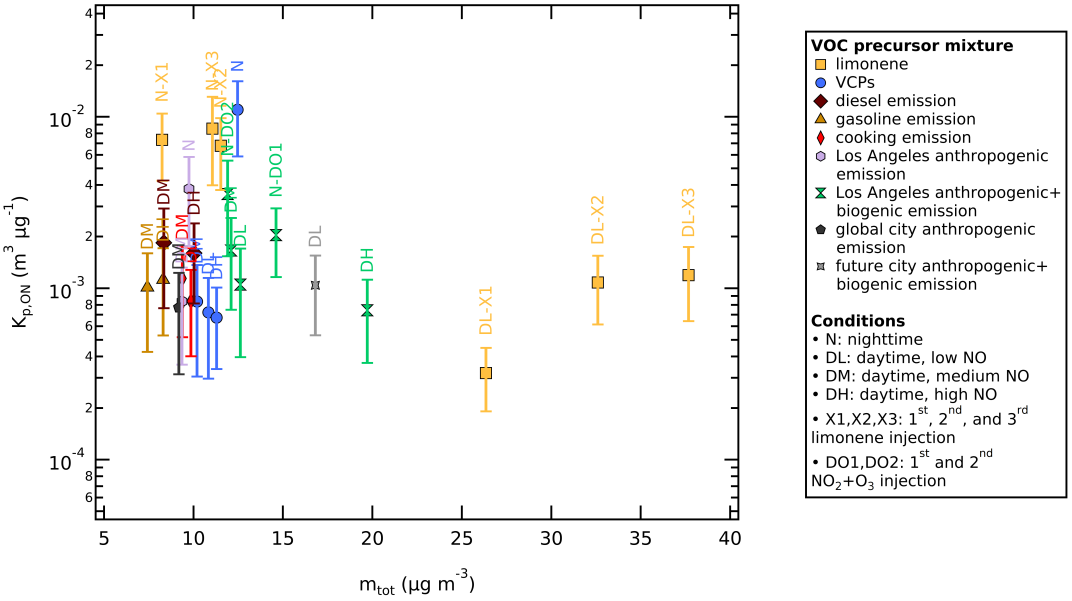

Figure S7. Scatter plot of $K_{\mathrm{p,ON}}$ against the total absorptive mass of PM at equilibrium (m_{tot}) for various urban VOC-NO_x mixture experiments, color-coded by VOC precursor mixture. The whiskers represent ± 46 % uncertainty (one standard deviation) of the bulk $K_{\mathrm{p,ON}}$. The plot suggests that differences in $K_{\mathrm{p,ON}}$ (thus $C_{\mathrm{pON}}/C_{\mathrm{gON}}$) in this range of total absorptive mass are not simply driven by differences in m_{tot}.

References

Baylon, P., Jaffe, D., Wigder, N., Gao, H., and Hee, J.: Ozone enhancement in western US wildfire plumes at the Mt. Bachelor Observatory: The role of NOx, Atmospheric Environment, 109, 297–304, https://doi.org/10.1016/j.atmosenv.2014.09.013, 2015.

Berndt, T.: Peroxy Radical Processes and Product Formation in the OH Radical-Initiated Oxidation of α-Pinene for Near-Atmospheric Conditions, The Journal of Physical Chemistry A, 125, 9151–9160, https://doi.org/10.1021/acs.jpca.1c05576, 2021.

Cai, R., Li, Y., Clément, Y., Li, D., Dubois, C., Fabre, M., Besson, L., Perrier, S., George, C., Ehn, M., Huang, C., Yi, P., Ma, Y., and Riva, M.: Orbitool: a software tool for analyzing online Orbitrap mass spectrometry data, Atmospheric Measurement Techniques, 14, 2377–2387, https://doi.org/10.5194/amt-14-2377-2021, publisher: Copernicus GmbH, 2021.

Day, D. A., Campuzano-Jost, P., Nault, B. A., Palm, B. B., Hu, W., Guo, H., Wooldridge, P. J., Cohen, R. C., Docherty, K. S., Huffman, J. A., de Sá, S. S., Martin, S. T., and Jimenez, J. L.: A systematic re-evaluation of methods for quantification of bulk particle-phase organic nitrates using real-time aerosol mass spectrometry, Atmospheric Measurement Techniques, 15, 459–483, https://doi.org/10.5194/amt-15-459-2022, 2022.

Eisele, F. L. and Tanner, D. J.: Measurement of the gas phase concentration of H_2SO_4 and methane sulfonic acid and estimates of H_2 SO_4 production and loss in the atmosphere, Journal of Geophysical Research: Atmospheres, 98, 9001–9010, https://doi.org/10.1029/93JD00031, 1993.

Gao, L., Zgheib, I., Stergiou, E., Carstens, C., Sari Doré, F., Dupanloup, M., Bourgain, F., Perrier, S., and Riva, M.: Characterization of the newly designed wall-free particle evaporator (WALL-E) for online measurements of atmospheric particles, https://doi.org/10.5194/amt-18-5087-2025, 2025.

González-Sánchez, J. M., Brun, N., Wu, J., Morin, J., Temime-Roussel, B., Ravier, S., Mouchel-Vallon, C., Clément, J.-L., and Monod, A.: On the importance of atmospheric loss of organic nitrates by aqueous-phase OH oxidation, Atmospheric Chemistry and Physics, 21, 4915–4937, https://doi.org/10.5194/acp-21-4915-2021, 2021.

Ji, Y., Huey, L. G., Tanner, D. J., Lee, Y. R., Veres, P. R., Neuman, J. A., Wang, Y., and Wang, X.: A vacuum ultraviolet ion source (VUV-IS) for iodide–chemical ionization mass spectrometry: a substitute for radioactive ion sources, Atmospheric Measurement Techniques, 13, 3683–3696, https://doi.org/10.5194/amt-13-3683-2020, 2020.

Junninen, H., Ehn, M., Petäjä, T., Luosujärvi, L., Kotiaho, T., Kostiainen, R., Rohner, U., Gonin, M., Fuhrer, K., Kulmala, M., and Worsnop, D. R.: A high-resolution mass spectrometer to measure atmospheric ion composition, Atmospheric Measurement Techniques, 3, 1039–1053, https://doi.org/10.5194/amt-3-1039-2010, 2010.

Krechmer, J., Lopez-Hilfiker, F., Koss, A., Hutterli, M., Stoermer, C., Deming, B., Kimmel, J., Warneke, C., Holzinger, R., Jayne, J., Worsnop, D., Fuhrer, K., Gonin, M., and De Gouw, J.: Evaluation of a New Reagent-Ion Source and Focusing Ion–Molecule Reactor for Use in Proton-Transfer-Reaction Mass Spectrometry, Analytical Chemistry, 90, 12 011–12 018, https://doi.org/10.1021/acs.analchem.8b02641, 2018.

Lee, B. H., Lopez-Hilfiker, F. D., Mohr, C., Kurtén, T., Worsnop, D. R., and Thornton, J. A.: An Iodide-Adduct High-Resolution Time-of-Flight Chemical-Ionization Mass Spectrometer: Application to Atmospheric Inorganic and Organic Compounds, Environmental Science & Technology, 48, 6309–6317, https://doi.org/10.1021/es500362a, 2014.

Riva, M., Ehn, M., Li, D., Tomaz, S., Bourgain, F., Perrier, S., and George, C.: CI-Orbitrap: An Analytical Instrument To Study Atmospheric Reactive Organic Species, Analytical Chemistry, 91, 9419–9423, https://doi.org/10.1021/acs.analchem.9b02093, publisher: American Chemical Society (ACS), 2019.

Riva, M., Brüggemann, M., Li, D., Perrier, S., George, C., Herrmann, H., and Berndt, T.: Capability of CI-Orbitrap for Gas-Phase Analysis in Atmospheric Chemistry: A Comparison with the CI-APi-TOF Technique, Analytical Chemistry, 92, 8142–8150, https://doi.org/10.1021/acs.analchem.0c00111, publisher: American Chemical Society (ACS), 2020.

Takeuchi, M., Wang, Y., Nault, B. A., Chen, Y., Canagaratna, M. R., and Ng, N. L.: Evaluating the response of the Aerodyne aerosol mass spectrometer to monoterpene- and isoprene-derived organic nitrate standards, Aerosol Science and Technology, 58, 1371–1388, https://doi.org/10.1080/02786826.2024.2389183, 2024.

Winer, A. M., Peters, J. W., Smith, J. P., and Pitts, J. N.: Response of commercial chemiluminescent nitric oxide-nitrogen dioxide analyzers to other nitrogen-containing compounds, Environmental Science & Technology, 8, 1118–1121, https://doi.org/10.1021/es60098a004, 1974.

Worton, D. R., Moreno, S., O'Daly, K., and Holzinger, R.: Development of an International System of Units (SI)-traceable transmission curve reference material to improve the quantitation and comparability of proton-transfer-reaction mass-spectrometry measurements, Atmospheric Measurement Techniques, 16, 1061–1072, https://doi.org/10.5194/amt-16-1061-2023, 2023.

Wu, Y., Tillmann, R., Pfannerstill, E. Y., Khare, P., Marcillo Carolina, A., Grasse, A., Rohrer, F., Depp, C., Roska, M., Adam, M. G., Albertin, S., Asgher, R., Bannan, T. J., Barua, S., Bates, K. H., Bell, D. M., Bohn, B., Brown, S., Buchholz, A., Chen, Y., Cho, C., Coe, H., Coggon, M. M., Färber, M., Farhoudian, S., Fry, J. L., Fuchs, H., Graus, M., El Haddad, I., He, Q., Hohaus, T., Iyer, S., Karydis, V. A., Kumar, A., Leiminger, M., Liu, L., Matthews, E., McFiggans, G., Middlebrook, A. M., Müller, M., Nissine, A., Nölscher, A. C., Novelli, A., Nursanto,

F. R., Perrier, S., Prévôt, A. S. H., Pullinen, I., Pusfitasari, E. D., Reinecke, T., Rissanen, M., Riva, M., Robinson, M. A., Schobesberger, S., Stockwell, C. E., Top, J., Tsimpidi, A. P., Vinkvist, N., Voliotis, A., Wahner, A., Wang, Y., Wang, Y., Warneke, C., Wegener, R., Yang, B., and Gkatzelis, G. I.: Recreating the breath of cities in the atmospheric simulation chamber SAPHIR, *Environmental Science & Technology*, in review, 2026.

Xu, L., Coggon, M. M., Stockwell, C. E., Gilman, J. B., Robinson, M. A., Breitenlechner, M., Lamplugh, A., Crounse, J. D., Wennberg, P. O., Neuman, J. A., Novak, G. A., Veres, P. R., Brown, S. S., and Warneke, C.: Chemical ionization mass spectrometry utilizing ammonium ions (NH_4^+ CIMS) for measurements of organic compounds in the atmosphere, Atmospheric Measurement Techniques, 15, 7353–7373, https://doi.org/10.5194/amt-15-7353-2022, 2022.